

# **Techno-economic Modelling of Onshore Wind Power**

---



# **Techno-economic Modelling of Onshore Wind Power**

Center for Study of Science, Technology and Policy

November 2022

Designed and edited by CSTEP

### **Disclaimer**

While every effort has been made for the correctness of data/information used in this report, neither the authors nor CSTEP accepts any legal liability for the accuracy or inferences for the material contained in this report and for any consequences arising from the use of this material.

© 2022 Center for Study of Science, Technology and Policy (CSTEP)

Any reproduction in full or part of this publication must mention the title and/or citation, which is provided below.

**Contributors:** Dr N S Suresh and S M Revathy

(The author list provided assumes no particular order as every individual contributed to the successful execution of the project)

**This report should be cited as:** CSTEP. 2022. *Techno-economic modelling of onshore wind power*. (CSTEP-RR-2022-13).

November 2022

### **Center for Study of Science, Technology and Policy**

#### **Bengaluru**

18, 10<sup>th</sup> Cross, Mayura Street  
Papanna Layout, Nagashettyhalli  
RMV II Stage, Bengaluru 560094  
Karnataka (India)

#### **Noida**

1<sup>st</sup> Floor, Tower-A  
Smartworks Corporate Park  
Sector 125, Noida 201303  
Uttar Pradesh (India)

Tel.: +91 (80) 6690 2500

Email: [cpe@cstep.in](mailto:cpe@cstep.in)

# Acknowledgements

The authors are thankful to the CSTEP management for giving us the opportunity to conduct this study. The guidance and support from Mr Thirumalai N C, Sector Head of Strategic Studies, proved invaluable in completing the study.

We acknowledge the following former employees of CSTEP for their timely contribution and technical reviews: Milind Ravindranath and Dr Vinay Kandagal.

We also acknowledge the support from the Communication and Policy Engagement team of CSTEP.

Editorial support: Reghu Ram R

Graphical support: Pooja Senthil and Alok Kumar Saha

# Executive Summary

Renewable energy will play a crucial role in India's effort to become a net-zero emission nation by 2070. Among the major renewable energy sources available in India, the potential of wind energy is largely untapped. India has the fourth largest installed capacity of wind energy in the world, with the addition of 41 GW as of June 2022. However, this figure is quite low when we consider India's potential of 695.5 GW at 120 m hub height and 302 GW at 100 m hub height. To unlock the true potential of wind energy in India and generate power efficiently, current wind farm designs need to be optimised. Increasing the hub height and optimising the positioning of turbines are two options that play a huge role in efficient power generation and land utilisation.

In our study, we developed a techno-economic model of on-shore wind power to optimise wind farm designs. We designed a wind farm by optimising land to achieve higher electricity generation (higher capacity utilisation) using mathematical modelling. The Monte Carlo method was used to optimally position turbines for generating maximum annual power. *Indicative power*, a new concept, was used to minimise the simulation time while performing the optimisation. Indicative power estimation considers effective input values of wind speeds and wind directions instead of considering yearly data (effective data sets are calculated using the historical wind data). Wake effects were accounted for the modelling using various analytical techniques, viz the Jensen model, the Frandsen model, and the Bastankhah model.

Superposition techniques were used to account for the interaction of wake fields. Further, different shapes of land (square, triangle, rectangle, and circle) were examined while modelling and optimising the wind farm. Multiple runs of Monte Carlo simulation helped in identifying optimum positions of turbines. Finally, optimum positions of turbines were used to estimate the technical and economic performance of the plant, considering hourly simulation.

A case study is presented to discuss the results of the application of the developed model in designing a wind farm in Nagercoil. For this, a farm capacity of 36 MW with 10 wind turbines of equal hub heights was chosen. The results indicate that the model optimised wind turbine positions by reducing the wake losses from 7% (initial layout) to 3% (optimised layout) and generated electricity at a capacity utilisation factor of 56%. The results have been validated using the System Advisor Model (SAM). The developed model reduces wake losses compared to SAM and generates more electricity.

A web-based graphical user interface (GUI) tool was developed from this model for performing land optimisation and techno-economic analyses for a range of inputs. Users can provide customised inputs (land area or farm capacity, resource data of a chosen location, land shape, topography characteristics, turbine sizes, etc.) and simulate the tool. The tool uses the Monte Carlo method to optimise turbine positions by minimising wake losses and maximising electricity generation. The tool provides a variety of results, including resource characteristics, turbine characteristics, wake losses, wind farm optimisation, and economic insights to optimise a wind farm.

# Contents

|  |    |
|--|----|
| 1. Introduction.....   | 15 |
| 2. Modelling Approach.....   | 17 |
| 2.1. Resource assessment.....  | 17 |
| 2.2. Indicative power of the wind farm.....                          | 19 |
| 2.3. True power of the wind farm.....                                | 19 |
| 2.4. Wake modelling.....   | 20 |
| 2.4.1. Understanding wake.....                                       | 21 |
| 2.4.2. Analytical wake models.....                                   | 23 |
| 2.5. Overlap.....  | 27 |
| 2.6. Identification of neighbours and rotation of turbine plane..... | 29 |
| 2.7. Superposition.....  | 30 |
| 2.7.1. Geometric sum.....  | 30 |
| 2.7.2. Linear sum.....   | 31 |
| 2.7.3. Sum of squares.....   | 31 |
| 2.7.4. Energy balance.....   | 31 |
| 2.8. Layout optimisation.....  | 32 |
| 2.8.1. Layout geometries.....  | 32 |
| 2.8.2. Representative power calculation.....                         | 34 |
| 2.8.3. Wind farm layout optimisation.....                            | 34 |
| 2.9. Overall flow chart.....   | 37 |
| 3. Results and Analysis: A Case Study.....                           | 39 |
| 3.1. Wind resource assessment.....                                   | 39 |
| 3.2. Comparative analysis of different wake models.....              | 41 |
| 3.3. Initial turbine layout configuration.....                       | 43 |
| 3.4. Approach for the displacement of turbines.....                  | 44 |
| 3.5. Optimised farm layout.....                                      | 45 |
| 3.6. Comparison of Initial and Optimised Layout with MC runs.....    | 46 |

|       |  |    |
|-------|--|----|
| 3.7.  | Comparison of wake recovery .....                                  | 48 |
| 3.8.  | Annual electricity of the optimised wind farm .....                | 49 |
| 3.9.  | Economic analysis.....   | 49 |
| 3.10. | Validation of the current model with the System Advisor Model..... | 50 |
| 4.    | Graphical user interface web tool.....                             | 53 |
| 5.    | Conclusion.....  | 57 |
| 6.    | References.....  | 58 |

# Tables

|   |    |
|---|----|
| Table 1: Classification of wind directions.....         | 17 |
| Table 2: Wind speed bins .....                          | 18 |
| Table 3: Wind direction sectors and their weights ..... | 41 |
| Table 4: Model validation with SAM.....                 | 50 |

# Figures

|  |    |
|--|----|
| Figure 1: Installed capacity of non-fossil fuels in India .....  | 16 |
| Figure 2: Classification of wind direction sectors.....  | 18 |
| Figure 3: The power curve of a 3.6 MW wind turbine .....   | 20 |
| Figure 4: Actuator disk model of the wind stream .....   | 21 |
| Figure 5: Illustration of wake expansion in the Jensen model.....  | 23 |
| Figure 6: The illustration of wake expansion in the Frandsen model .....   | 25 |
| Figure 7: Illustration of the Bastankhah model .....   | 26 |
| Figure 8: The axial view of various modes of wake field interaction of upstream and downstream turbines .....    | 27 |
| Figure 9: The interaction of wake field and rotor based on the intersection of circles .....                     | 28 |
| Figure 10: The overlap fraction of downstream turbines .....   | 29 |
| Figure 11: Identified turbine neighbours in the wind farm layout for a wind direction of $270^{\circ}$           | 30 |
| Figure 12: Wake expansion among four turbines.....   | 32 |
| Figure 13: Illustration of the square layout with an example.....  | 33 |
| Figure 14: Illustration of the rectangle layout with an example.....   | 33 |
| Figure 15: Illustration of the isosceles triangle layout with an example .....                                   | 34 |
| Figure 16: Illustration of the circle layout with an example.....  | 34 |
| Figure 17: The trial displacement of a turbine within the layout.....  | 36 |
| Figure 18: Different MC steps and associated trial displacements.....  | 36 |
| Figure 19: Acceptance criteria of trial displacements.....   | 36 |
| Figure 20: Overall flow chart of the MC simulation .....   | 37 |
| Figure 21: Wind rose diagram for Nagarcoil.....  | 40 |
| Figure 22: The wind flow distribution in different wind sectors .....  | 40 |
| Figure 23: Wind speed bin weights in selected sectors.....   | 41 |
| Figure 24: Comparison of different wake models to examine the regain velocity for an inflow wind of 14 m/s ..... | 42 |
| Figure 25: Comparison of different wake models to examine the regain velocity for an inflow wind of 24 m/s ..... | 42 |
| Figure 26: Initial layout of turbines.....   | 43 |
| Figure 27: Position of turbines at MC Cycle 1.....   | 44 |
| Figure 28: Position of turbines at MC Cycle 9.....   | 44 |
| Figure 29: Position of turbines at MC Cycle 10 .....   | 45 |
| Figure 30: Optimised farm layout.....  | 45 |

|  |    |
|--|----|
| Figure 31: Indicative power of the initial and final layout of MC Cycle 1.....                         | 46 |
| Figure 32: Indicative layout power for 100 MC cycles.....  | 46 |
| Figure 33: Turbine positioning of initial (a) and optimised layouts (b) for the first MC run .....     | 47 |
| Figure 34: Turbine positioning of the initial (a) and optimised layout (b) for the second MC run ..... | 47 |
| Figure 35: Indicative power output throughout the MC cycles for the second MC run .....                | 48 |
| Figure 36: Wake recovery of the initial layout.....  | 48 |
| Figure 37: Wake recovery of the optimised layout .....   | 49 |
| Figure 38: Annual electricity generated by the turbines from the initial and optimised layouts         | 49 |
| Figure 39: The sample layout from the current model.....   | 51 |
| Figure 40: Layout of the sample farm from the SAM model.....   | 52 |
| Figure 41: Wind farm layout from SAM for 13 turbines .....   | 52 |
| Figure 42: The sample screen of a resource assessment in the web tool .....                            | 53 |
| Figure 43: The sample screen of turbine characteristics in the web tool.....                           | 53 |
| Figure 44: The sample screen of the wind farm layout in the web tool.....                              | 54 |
| Figure 45: Losses and other wind characteristics incorporated in the tool .....                        | 54 |
| Figure 46: Economic model in the tool.....   | 55 |

## Abbreviations

|      |                                      |
|------|--------------------------------------|
| CFD  | Computational fluid dynamics         |
| GA   | Genetic algorithm                    |
| kW   | Kilowatt                             |
| MCO  | Monte Carlo optimisation             |
| MW   | Megawatt                             |
| MWh  | Megawatt hour                        |
| NREL | National Renewable Energy Laboratory |
| PSO  | Particle swarm algorithm             |
| RE   | Renewable energy                     |
| SAM  | System Advisor Model                 |
| TMY  | Typical meteorological year          |
| WPD  | Wind power density                   |

## Nomenclature

|                      |  |
|----------------------|--|
| $a$                  | Axial induction factor   |
| $A_1$                | Area of cross section of $C_1$                                       |
| $A_2$                | Area of cross section of $C_4$                                       |
| $A_r$                | Area of the wind turbine rotor                                       |
| $C_1, C_2, C_3, C_4$ | Different cross sections in the actuator disk model in a wind stream |
| $C_p$                | Coefficient of power   |
| $C_T$                | Coefficient of thrust  |
| $d_i$                | Direction weights for each wind sector                               |
| $D_r$                | Turbine rotor diameter   |
| $i$                  | Wind sector numbers (1 to 16)  |
| $j$                  | Wind speed bin numbers (0 to 9)                                      |

|               |   |
|---------------|---|
| $N$           | Number of days in a year  |
| $n_i$         | Number of values in each wind sector                            |
| $N_{tur}$     | Number of turbines  |
| $P$           | Total wind farm layout power                                    |
| $p_0$         | Ambient pressure  |
| $p_d$         | Pressure at cross section $C_3$ in the actuator disk model      |
| $P_{in}$      | Power available in the free stream wind                         |
| $P_{N,i,j}$   | Power corresponding to the representative wind speed            |
| $p_u$         | Pressure at cross section $C_2$ in the actuator disk model      |
| $r_2$         | Radius of the near wake   |
| $r_r$         | Wind turbine rotor radius                                       |
| $R_{rad}$     | Rotor radius of the downstream turbine                          |
| $s_{i,j}$     | Wind speed weights at each sector                               |
| $T$           | Thrust force  |
| $T_1$         | Turbine 1   |
| $T_2$         | Turbine 2   |
| $T_3$         | Turbine 3   |
| $T_4$         | Turbine 4   |
| $T_{max}$     | Maximum thrust force  |
| $v_0$         | Inflow wind speed   |
| $v_x$         | Regain wind speed at the farthest wake                          |
| $W_{rad}$     | Wake field radius of the upstream turbine                       |
| $x$           | Distance between the upstream and downstream wind turbine       |
| $x_1$         | Distance between the rotor and the near wake region             |
| $x_2$         | Distance between the near wake and far wake regions             |
| $\alpha$      | Slope of wake expansion from the near wake to the farthest wake |
| $\alpha_{in}$ | Slope of wake expansion from the rotor to the near wake         |
| $\rho$        | Density of air  |





# 1. Introduction

The Indian electricity sector has seen remarkable contributions from the renewable energy (RE) sector in recent years. Depletion of conventional energy sources and adverse effects associated with the utilisation of such resources have driven significant RE penetration, and recent stats on installed capacity and its electricity share from non-fossil fuels confirm this trend (see Figure 1). India is aiming to add a non-fossil energy capacity of 500 GW by 2030, and wind energy could play a huge role in achieving this target. It is a major renewable energy resource that contributes substantially to electricity generation in India, with 100% of the share coming from onshore wind at present. However, the current installed capacity of wind energy (onshore) is low compared to the country's potential of 695.5 GW at 120 m hub height and 302 GW at 100 m hub height.

Also, wind farms require huge tracts of land. A one square kilometre land area can house only a 5–9 MW wind farm (though the footprint area required is just 3%–4%). Therefore, land resources should be used carefully when wind farms are installed. The right positioning of wind turbines is critical to utilise land resources optimally and generate power efficiently to achieve national targets. The current study aimed at developing a model to design a wind farm that generates maximum power with efficient utilisation of land resources. The model considered engineering and economic aspects in detail to optimise the wind farm.

Relevant literature was reviewed prior to developing the model. Various studies have attempted the optimisation of wind farms (Baker, Stanley, Thomas, Ning, and Dykes, 2019; Balasubramanian, Thanikanti, Subramaniam, Sudhakar, and Sichilalu, 2020; Gebraad et al., 2016; Gualtieri, 2019; Niayifar and Porté-Agel, 2015). Baker et al. proposed gradient-based optimisation methods and analysed physics and strategies related to wind turbines. Balasubramanian et al. compared different approaches to wind farm optimisation based on various parameters such as technologies, convergence speed computation, and complexity. Gebraad et al. coupled wind farm controls and layout positioning to establish a new engineering optimisation possibility. Gualtieri analysed the possible combinations of turbine placement by considering site specifications and wind characteristics through an irregularly staggered turbine array configuration. Niayifar and Porté-Agel performed a detailed accounting of wake interaction in wind farms by considering the boundary layer turbulence and its comparison with a large eddy simulation to understand the associated energy deficit. All these works present different approaches to cost-efficient optimisation of wind farms and associated power generation.

The current study evaluated different analytical wake modelling approaches and land optimisation techniques for designing a wind farm. It broadly covers the following:

- Wind resource assessment
- Analytical wake models
- Turbine power characteristics
- Overlap of wakes and effective incoming wind speed to each turbine in a farm
- Optimisation of the wind farm for maximum energy output using the Monte Carlo method
- Economic modelling
- Results and analysis of key techno-economic indicators using a case study
- Web-based graphical user interface (GUI) tool



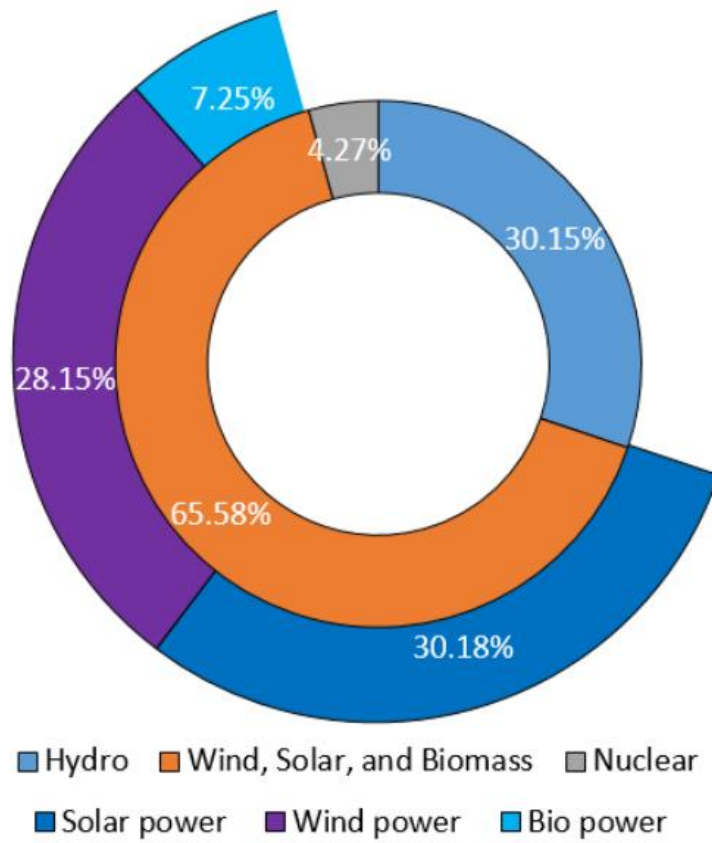
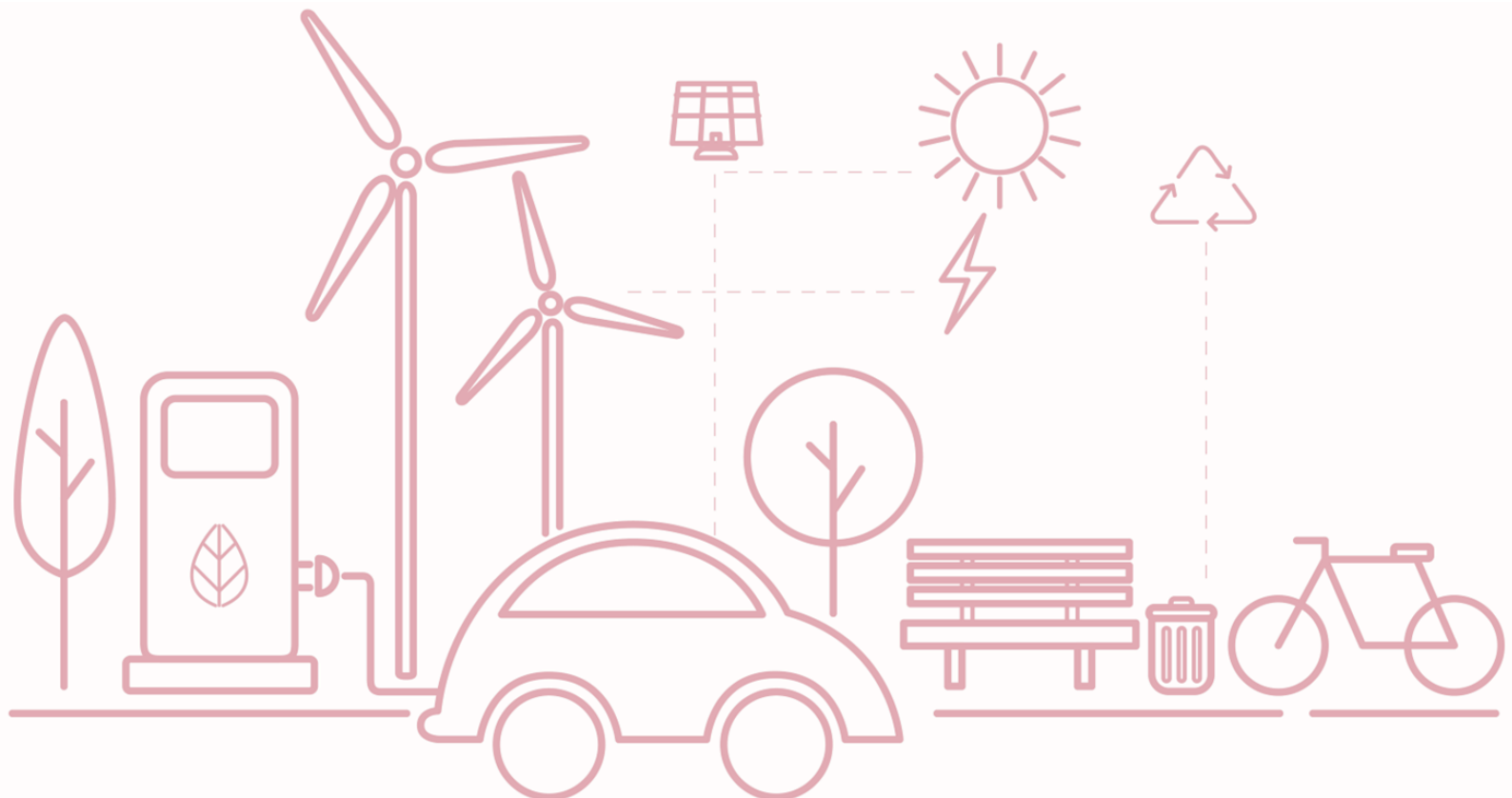


Figure 1: Installed capacity of non-fossil fuels in India



## 2. Modelling Approach

This section covers the modelling approach for designing a wind farm for a given plant capacity or a given land area.

### 2.1. Resource assessment

Assessment of wind resource at a given location is essential to estimate the potential of a site and design and operate a wind farm. The assessment includes the analysis of two important parameters of a wind resource at a given hub height: wind speed and wind direction. These parameters and wake modelling help in siting wind turbines at right locations in a wind farm.

Resource data are typically available from three sources: in-situ measurements, satellite images, and analytical/mathematical methods. The time interval of such data can be in seconds, minutes, or hours. Finer temporal resolution data help in building a better meteorological system as micro-scale changes in a system can be captured accurately. The current study considered five-minute interval data for the wind resource assessment. The performance of a wind turbine depends on wind speed and wind direction. Resource data from a typical meteorological year, with 8760 values of wind direction and wind speed each, were considered in the study. To minimise the computational time for optimising the wind farm, the study considered 16 sectors of wind direction and nine wind speed bins while optimising land for a given plant capacity. Specific nomenclature was assigned to indicate the 16 sectors of wind direction, and anticlockwise direction was considered (see Table 1 and Figure 2).

Table 1: Classification of wind directions

| Sector no. | Wind direction | Sector no. | Wind direction |
|------------|----------------|------------|----------------|
| Sector 1   | N              | Sector 9   | S              |
| Sector 2   | NNW            | Sector 10  | SSE            |
| Sector 3   | NW             | Sector 11  | SE             |
| Sector 4   | WNW            | Sector 12  | ESE            |
| Sector 5   | W              | Sector 13  | E              |
| Sector 6   | WSW            | Sector 14  | ENE            |
| Sector 7   | SW             | Sector 15  | NE             |
| Sector 8   | SSW            | Sector 16  | NNE            |



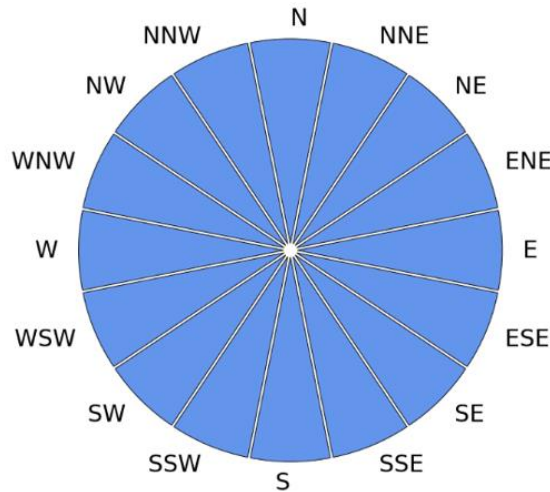


Figure 2: Classification of wind direction sectors

The study considered a total of nine wind speed bins (see Table 2): eight between cut-in wind speed and rated wind speed and one between rated wind speed and cut-out wind speed. Wind turbines generate power between cut-in (~3 m/s) and cut-out wind (~25 m/s) speeds, and they receive wind from directions between 0° and 360°.

Table 2: Wind speed bins

| Wind speed (m/s)  | Bin |
|-------------------|-----|
| 3 to 4.1875       | 1   |
| 4.1875 to 5.375   | 2   |
| 5.375 to 6.5625   | 3   |
| 6.5625 to 7.75    | 4   |
| 7.75 to 8.9375    | 5   |
| 8.9375 to 10.125  | 6   |
| 10.125 to 11.3125 | 7   |
| 11.3125 to 12.5   | 8   |
| 12.5 to 25        | 9   |

The weightage of wind direction and wind speed (based on typical meteorological year data) was introduced to account for their effect while optimising the wind farm (better positioning of wind turbines) at a given location.

The following steps were considered while estimating the wind direction weight:

1. Read input values of wind direction (8760 values in an hourly weather data file)

2. Estimate the effective values of wind direction ( $\leq$ cut in wind speed and  $\geq$ cut out wind speed),  $N$  out of 8760 values
3. Estimate the number of values of wind direction in each sector,  $n_i$  ( $i=1$  to 16)
4. Estimate the direction weight in each ( $i^{\text{th}}$ ) sector

$$d_i = n_i/N, \quad (2.1.1)$$

where  $i = i^{\text{th}}$  wind direction sector.

The following steps were considered while estimating the wind speed weight:

1. Segregate the 8760 values of wind speeds according to wind direction sectors (16 sectors)
2. Classify wind speeds in each sector into nine bins (refer to Table 2; eight bins from cut-in speed to rated speed and one bin from rated to cut-out speed)
3. Estimate the weight of wind speed in each sector as follows:

$$s_{ij} = \frac{n_{ij}}{n_i}, \quad (2.1.2)$$

where  $j = 1$  to 9 (represents wind speed bins).

The effective weight of resource represents the weightage of wind direction and wind speed. This was estimated for each wind direction sector as follows:

$$\text{Effective weight} = d_i \times \sum_{j=1}^9 s_{i,j} \quad \forall i = 1 \text{ to } 16. \quad (2.1.3)$$

## 2.2. Indicative power of the wind farm

*Indicative power* is a term used in the study to optimise the wind farm based on representative wind speed (average of the wind speed in each speed bin), wind direction, and corresponding weights associated. The available wind speed for each turbine in the wind farm differs as per the wake interaction among turbines at any instant.

The uncertainty in wind direction and speed was addressed through their weights while estimating the indicative power of the wind farm. The indicative layout power is estimated as

$$P = \sum_{N=1}^{N_{tur}} \left( \sum_{i=1}^{16} d_i \times \sum_{j=1}^9 s_{i,j} \times P_{N,i,j} \right), \quad (2.2.1)$$

where  $P_{N,i,j}$  indicates the power corresponding to the representative wind speed (average of each velocity bin). Power from the representative wind speed was calculated using the power curve information of the selected wind turbine (see Section 2.3).

## 2.3. True power of the wind farm

The layout was optimised (placing turbines at optimised positions) considering the indicative power using the Monte Carlo method. True power from optimised positions of turbines was estimated with hourly resource data from over a year and power curve data of a selected size of the turbine. The power performance of the chosen size of the turbine varies from one manufacturer to other. The study considered a 3.6 MW turbine from Siemens Gamesa (see



Figure 3 for the power curve) for the representative case (the web tool provides a list of various turbines from different manufacturers). The turbine started generating power from a wind speed of 3 m/s (cut-in wind speed) and met the design turbine power at ~12 m/s (rated wind speed). From 12 m/s to 25 m/s (cut-out) of wind speed, the turbine generated only the design turbine power irrespective of the increase in wind speed. Beyond the cut-out wind speed, the turbine went to the stow position (generated no power) because of operational challenges.

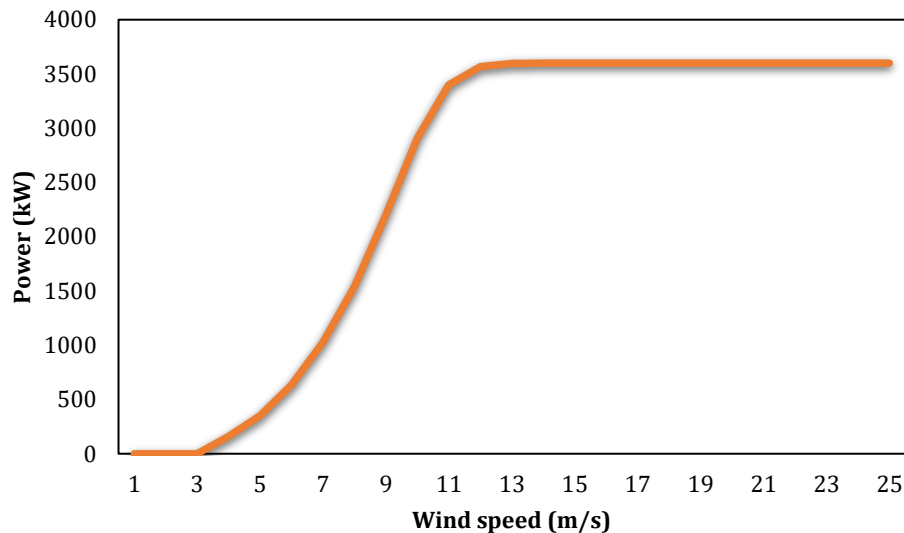


Figure 3: The power curve of a 3.6 MW wind turbine

## 2.4. Wake modelling

When wind flows across a rotor, an aerodynamic wake region is produced in its downstream. The wake region is associated with velocity deficit, differential pressure, and increased turbulence along its expanded area (Charhouni, 2015; Göçmen et al., 2016; Tong et al., 2012). The decreased wind speed and increased turbulence impact neighbouring turbines. Two major effects caused by wakes are the increase in mechanical loads and the decrease in energy output from turbines. To avoid this, turbines must be positioned at optimal distances to each other in a given layout.

Wake modelling helps in optimum positioning of turbines, enhancing the performance of a wind farm. There are two general approaches considered for developing the wake model: mathematical/analytical and computational fluid dynamics (CFD). Some of the analytical approaches are the Jensen model, the Frandsen model, Bastankhah model and the Ishihara model. CFD methods consider complex algorithms (FUGA and EllipSys3D) predominantly using Navier–Stokes equations (Göçmen et al., 2016). This complex algorithm accounts for various uncertain atmospheric parameters. CFD-based methods are more accurate as they solve the wake effect by considering various characteristics of uncertain weather and climate parameters than simple mathematical approaches. However, CFD models require high-end computational devices. Further, the wind farm model must undergo several runs accounting for the wake effect to arrive at the optimum outcome. Overall, CFD models are expensive and time-intensive. On the other hand, mathematical approaches are simple (neither expensive nor time-intensive) though their accuracy is less compared to CFD methods. The current



study used Jensen's wake model to assess the wake impact on wind farm performances. Before delving into these specific models, the general wake aspects are discussed below.

### 2.4.1. Understanding wake

Wake is a low-frequency meandering wind that has lower speed and higher turbulence compared to the free-stream wind (Sizhuang & Youtong, 2014). It forms downstream behind a turbine when the turbine absorbs some of the energy from the free-stream wind. The lower wind speeds due to wake affect the power production from a wind farm and add a mechanical load to turbine blades, thereby reducing life. An in-depth understanding of a wake field (combination of wakes) is important to study these aspects and design an optimised wind farm. Figure 4 illustrates a rotor and the boundary layer of a wind stream. The associated model considers no cross flow of wind from the outer body to the stream tube cross section. Further, a steady flow is assumed within the tube. The rotor of the turbine has been considered as an infinitesimally thick actuator disk that reduces the momentum of the axial wind.

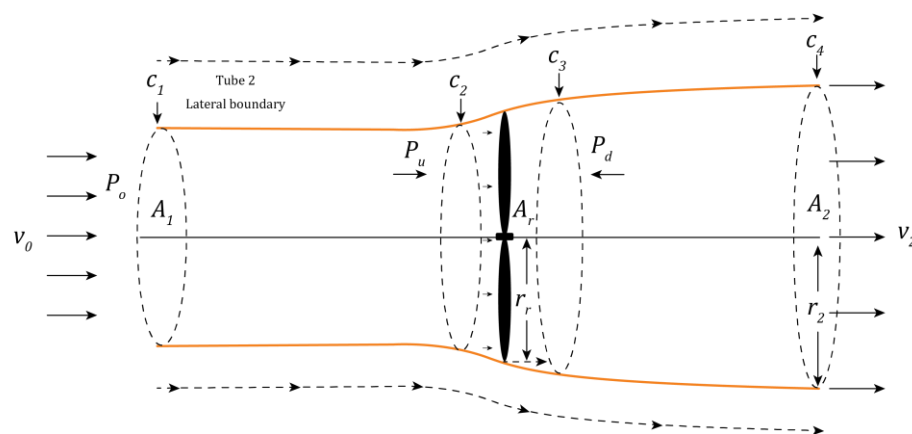


Figure 4: Actuator disk model of the wind stream

The cross section is divided into two tubes: Tube 1 and Tube 2 (see Figure 4). The upstream tube has a small cross section, and the downstream tube has a large cross section. The lateral boundary of Tube 1 touches the actuator disk.  $C_1$ ,  $C_2$ ,  $C_3$ , and  $C_4$  are the four cross sections in the stream where wind is distributed at varying speeds. The cross section  $C_2$  is right in front of the actuator disk, and  $C_3$  is behind the disk.  $A_1$ ,  $A_r$ , and  $A_2$  are the cross-sectional areas of  $C_1$ , the actuator disk (rotor), and  $C_4$ , respectively. The wind speed at  $C_1$ ,  $C_2$ ,  $C_3$ , and  $C_4$  cross sections are  $v_0$ ,  $v_1$ ,  $v_1$ , and  $v_2$ , respectively. The whole cross section from the rotor to  $C_4$  is considered the near-wake region. The overall cross section is assumed to be characterised by equal ambient pressure ( $p_0$ ) on both sides of the tube. Here,  $r_2$  is considered the downstream wake radius at a distance of  $x_1$  from the rotor (the length of the near-wake region). The key parameters used in the wake modelling are discussed in the next section.

#### 2.4.1.1. Mass flow rate

As indicated earlier, when the free-stream wind passes through the rotor, a part of it is



extracted by the rotor, decreasing wind speed in its immediate downstream. The axial induction factor captures this variation of speed between the free-stream wind and the immediate downstream wind. This is defined as

$$a = \frac{v_0 - v_1}{v_0}. \quad (2.4.1)$$

Under ideal conditions, the value of the induction factor is 1/3. This axial induction factor can be related to the power generated by the turbine (the wind speed at the rotor,  $v_0$ , determines the power from the turbine). If  $a = 1$ , the power generated by the turbine is zero as there is no wind flow through the blades of the turbine. If  $a = 0$ , no power is generated from the turbine because the kinetic energy before and after the turbine blades remains unchanged. This condition violates momentum conservation as the rotor does not impact the wind flow through its thrust force.

#### 2.4.1.2. Thrust force

Wind turbines generate power only when there are differential speeds of wind across the rotor in upward and downward directions. The change in wind speeds across the rotor causes differential pressure, which helps in the rotation of blades through lift force (drag is small) and thrust. The rotor extracts kinetic energy, reduces wind speed, and loses part of the wind momentum. The thrust force of the rotor is equal to this lost momentum of the wind. Pressure parameters can also be used to represent momentum. It can be inferred from Figure 4 that the pressure acting on  $C_1$  and  $C_4$  are same though the cross-sectional area differs. The thrust force is given by

$$T = \frac{1}{2} \rho (v_0^2 - v_2^2) A_r. \quad (2.4.2)$$

The thrust coefficient is defined as the ratio of force applied on the rotor by the wind and the maximum force carried by the free-stream wind. It is given by

$$C_T = \frac{T}{T_{max}}. \quad (2.4.3)$$

This has been further simplified in terms of the axial induction factor using the following equation:

$$C_T = 4a(1 - a). \quad (2.4.4)$$

#### 2.4.1.3. Power coefficient

Power is the quantity of work or energy extracted in a specific time. In the current case, the rotor extracts a fraction of energy from the free-stream wind and reduces the wind speed in its downstream. Power coefficient is defined as the ratio of power,  $P$ , extracted by the rotor to the power available in the free-stream wind,  $P_{in}$ :

$$C_P = \frac{P}{P_{in}}. \quad (2.4.5)$$

$C_P$  in terms of the axial induction factor is expressed as

$$C_P = 4a(1 - a)^2. \quad (2.4.6)$$



#### 2.4.1.4. Mass conservation

The farthest wake cross section is important to estimate the downstream wind speed. This is estimated considering the known parameters such as the rotor cross section and the axial induction factor.

According to the mass conservation law (see Figure 4), the downstream side of the stream tube for the rotor can be represented as

$$\rho A_r v_1 = \rho A_2 v_2 \text{ or } \rho \pi r_r^2 v_1 = \rho \pi r_2^2 v_2. \quad (2.4.7)$$

### 2.4.2. Analytical wake models

The analytical models used in the study are discussed in this section.

#### 2.4.2.1. The Jensen wake model

The Jensen wake model is a popular analytical model used in assessing the wake field associated with a wind turbine. The basis of the Jensen model is the actuator disk theory (Jensen, 1983; Tong, Chowdhury, Zhang, and Messac, 2012). The model assumes that the far wake expands linearly from the rotor (see Figure 5). The  $x_1$  regime indicates the nearest wake and the  $x_2$  regime indicates the farthest wake (Sizhuang and Youtong, 2014).

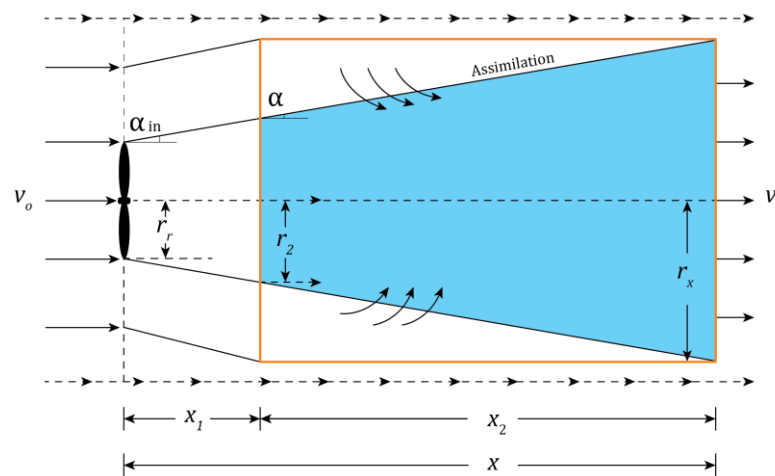


Figure 5: Illustration of wake expansion in the Jensen model

The control volume of the farthest wake is represented as a trapezoid with a blue shade. This model does not account for wake expansion from the rotor to the nearest wake. This is because the wind speed in the immediate downstream of the rotor is assumed to be the same as the upstream side of the rotor. Also, no assimilation of external wind happens in this region. In other words, the wake field would not have external disturbances from the rotor to the nearest wake. The model assumes that every cross section in the wake field expands linearly from the nearest wake to the farthest wake. Jensen considered four different theories while developing the wake model (Zhang and Wang, 2009).



**Version 1:** In this version, the control volume includes wake expansion from the rotor to the farthest wake (indicated as a trapezoid with a blue shade in Figure 5). The wake velocity at the farthest downstream is given by

$$v_x = \left[ 1 - \frac{2a}{(1 + 2\alpha(\frac{x}{D_r}))^2} \right] v_0, \tag{2.4.8}$$

where

$\alpha$ = slope of wake expansion,

$D_r$ = rotor diameter,

and

$x$  = distance between the upstream and downstream turbine (assuming the next turbine is located at the farthest wake position from the base turbine).

**Version 2:** The wake expands from the rotor in two different linear ways:

- (1) a slope of  $\alpha_0$  from the rotor to the nearest wake with a distance of  $x_1$
- (2) a slope of  $\alpha_1$  from the nearest wake to the farthest wake with a distance of  $x_2$

However, this model does not account for wake expansion from the rotor to the nearest wake. The region between the nearest wake and farthest wake is considered in this version. This is because the wind speed in the immediate downstream of the rotor is assumed to be the same as the upstream side of the rotor. Also, no assimilation of external wind happens in this region. In other words, wake effect is negligible from the rotor to the nearest wake. The model assumes that every cross section in the wake field expands linearly from the nearest wake to the farthest wake. The control volume is represented as a trapezoid with a blue shade (see Figure 5).

The regained wind speed at the farthest wake region is given by

$$v_x = \left[ 1 - \frac{2a}{(\frac{r_x}{r_2})^2} \right] v_0. \tag{2.4.9}$$

Here,  $r_x = r_2 + \alpha x_2$ .

**Version 3:** In this case, the model accounts for the linearity of wake expansion between Section 1 (the rotor and the nearest wake) and Section 2 (the nearest wake to the farthest wake). No assimilation happens in Section 1 (see Figure 5), whereas assimilation (mix of downstream wind and external wind) happens in Section 2 of the cross section. Therefore, the study assumes that the wake in Section 1 expands with an infinite slope ( $x_1$  becomes minimal).

The regained wind speed at the farthest downstream is given by

$$v_x = \left[ 1 - \frac{2a}{(1 + \alpha(\frac{x}{r_2}))^2} \right] v_0, \tag{2.4.10}$$

where  $r_2 = r_r \sqrt{\frac{1-a}{1-2a}}$ .



$$v_x = \left[ \frac{1}{2} + \frac{1}{2} \sqrt{1 - \frac{2C_T}{\left(\frac{r_2}{r_r}\right)^2 \left(0.8 + \frac{\alpha x}{r_2}\right)^2}} \right] v_0, \tag{2.4.14}$$

where  $r_2 = r_r \sqrt{\frac{1-a}{1-2a}}$  and  $C_T$  is the thrust coefficient.

2.4.2.3. The Bastankhah model

According to the theory of fluid dynamics, the flow in the downstream part of a bluff body follows the Gaussian profile. This is most commonly observed in wind tunnel experiments. The current model considers a similar approach for velocity deficit estimation downstream of the bluff body. Further, it holds both mass and momentum conservation. Figure 7 presents the control volume and wake expansion of the Bastankhah model.

The velocity deficit from the Bastankhah model is given by (Bastankhah & Porté-Agel, 2014)

$$\int \frac{\Delta v}{v_0} dA = 2\pi\epsilon^2 D_r^2 \left( 1 - \sqrt{1 - \frac{C_T}{8\epsilon^2}} \right), \tag{2.4.15}$$

where

$$\epsilon = 0.25\sqrt{\beta}, \quad \beta = \frac{1 + \sqrt{1 - C_T}}{2\sqrt{1 - C_T}}, \quad \text{and } D_r = \text{rotor diameter.}$$

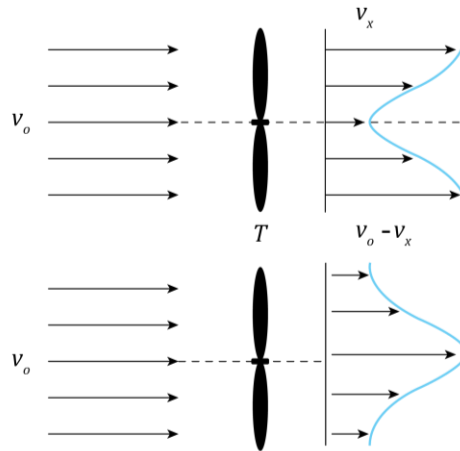


Figure 7: Illustration of the Bastankhah model

After estimating the wake width and velocity deficit (between two turbines) using one of the analytical wake models, multiple wake interactions were accounted for to estimate the overall impact of the wind farm. Major factors considered to estimate the total power output are as follows:

- the overlap of wake fields,
- change in the wake field interaction between turbines as the wind direction changes, and
- the superposition of turbine power output.

## 2.5. Overlap

As mentioned earlier, wake formation happens downstream of a turbine. The position of the next turbine in its downstream can be completely or partially covered by the wake field, depending on the distance at which it is located. The downstream turbine can have no wake coverage if it is located at a farther distance. The downstream distance from the upstream turbine, wake width, and wind direction are all factors that come into play in such a scenario. Generally, analytical models account for the wake recovery by considering a complete wake field interaction of upstream and downstream turbines. The wake recovery or regained wind speed changes depending on the fraction of wake overlap on the downstream turbine. This effect has a direct impact on the power generation by targeted turbines.

Figure 8 shows different modes of wake interaction on the downstream turbine. The large circle represents the maximum possible wake field (generated in the downstream side of an upstream turbine), and the smaller one indicates the downstream rotor area. Red dots represent the centre of the wake and the rotor. Subplots 1, 2, and 3 represent a complete overlap of the wake field and the downstream rotor. Subplot 4 shows partial interaction and Subplots 5 and 6 show null interaction.

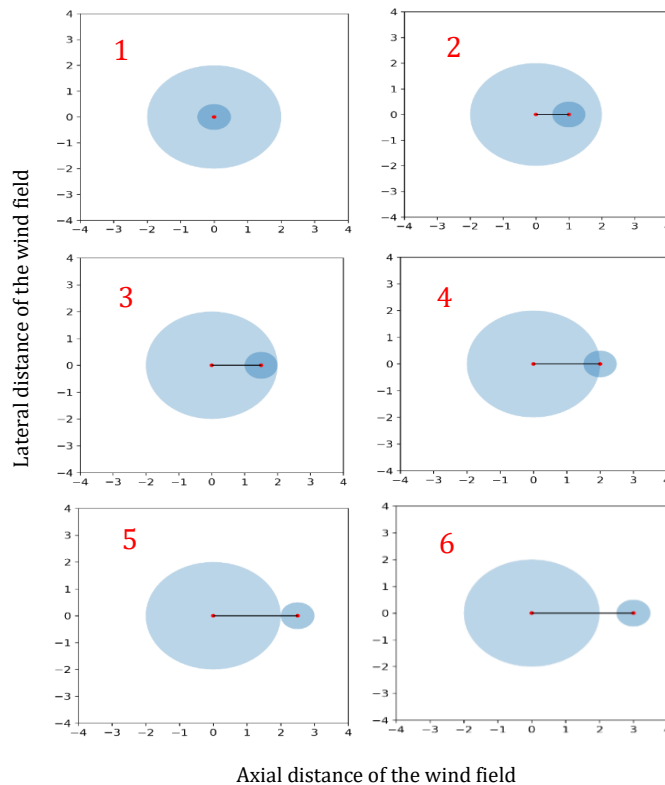


Figure 8: The axial view of various modes of wake field interaction of upstream and downstream turbines

The theory of intersection of circles was used to mathematically estimate the overlap fraction of wake in downstream turbines (Yang and Cho, 2019). Figure 9 indicates a representative interaction of the wake created by an upstream turbine and the rotor of a downstream turbine.  $A_1$  and  $A_2$  represent the fraction of the intersected area of the extended wake field of the upstream turbine and the area of the rotor in the downstream turbine.



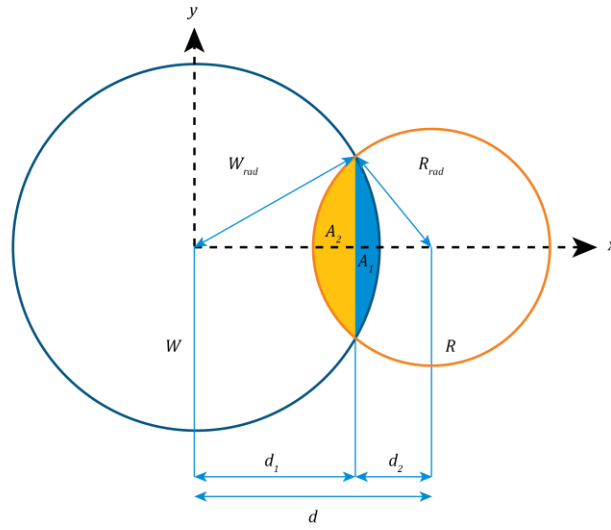


Figure 9: The interaction of wake field and rotor based on the intersection of circles

According to Pythagoras theorem and similarity theory of triangles,

$$d_1 = \frac{W_{rad}^2 - R_{rad}^2 + d^2}{2d}, \tag{2.5.1}$$

$$A_{intersection} = A_1 + A_2, \text{ and} \tag{2.5.2}$$

$$A_{intersection} = W_{rad}^2 \cos^{-1}\left(\frac{d_1}{W_{rad}}\right) - d_1 \sqrt{W_{rad}^2 - d_1^2} + R_{rad}^2 \cos^{-1}\left(\frac{d_2}{R_{rad}}\right) - d_2 \sqrt{R_{rad}^2 - d_2^2}. \tag{2.5.3}$$

Equations 2.5.1, 2.5.2, and 2.5.3 are used to estimate the fraction of overlap of the rotor area with the wake field according to the interactions. The overlap fraction can be written as

$$\frac{A_{intersection}}{Rotor\ area} = \frac{A_{intersection}}{\pi R_{rad}^2}. \tag{2.5.4}$$

Figure 10 presents overlap fractions for the cases mentioned above. The value of the overlap fraction varies between 0 and 1. The value 0 indicates no overlap and 1 indicates complete overlap. A fractional value between 0 and 1 indicates partial overlap.

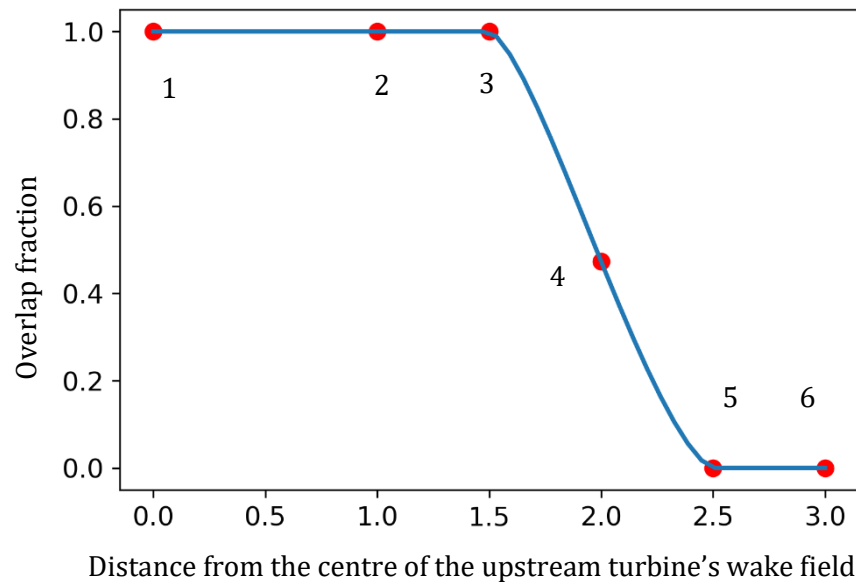


Figure 10: The overlap fraction of downstream turbines

A target turbine in a wind farm might interact with multiple wakes from different upstream turbines. Therefore, the overlap fraction has to be estimated for multiple wakes by considering appropriate upstream turbines according to the wind direction. These overlap fractions are cumulated and then multiplied with the velocity deficit (estimated using wake models) to estimate the overall velocity deficit at the targeted turbine. The overall velocity deficit at the targeted turbine is developed as

$$\text{Actual velocity deficit} = \frac{\text{Velocity deficit at the downstream turbine}}{\text{Overlap fraction}} \quad (2.5.5)$$

## 2.6. Identification of neighbours and rotation of turbine plane

All turbines in a wind farm are associated with the wake field caused by the surrounding turbines at any given wind direction. Downstream turbines that fall under the wake field of upstream turbines are considered neighbours of upstream turbines. Varying wind directions create new neighbours for turbines at any given instant. Overlap fractions and the power production from each turbine vary accordingly. Thus, identification of neighbours at each instant of time is important to estimate the true power production of the wind farm.

A Cartesian coordinate system is used to rotate the wind field plane according to the wind direction to identify neighbours. This implies that the coordinates of all turbines are changed to new coordinates according to the wind direction. The new coordinates are used to estimate the wake width of upstream turbines and identify neighbours.

An example is given below to illustrate the concept. As shown in Figure 11, Figure 10 turbines (labelled with numbers starting from 0 to 9) were located in a square-shaped wind farm. Neighbours of upstream turbines were identified for a given wind direction of 270°; for example, neighbour turbines for Turbine 9 are 4, 2, and 1. The number of neighbour turbines for each turbine is shown in panel b of the figure.



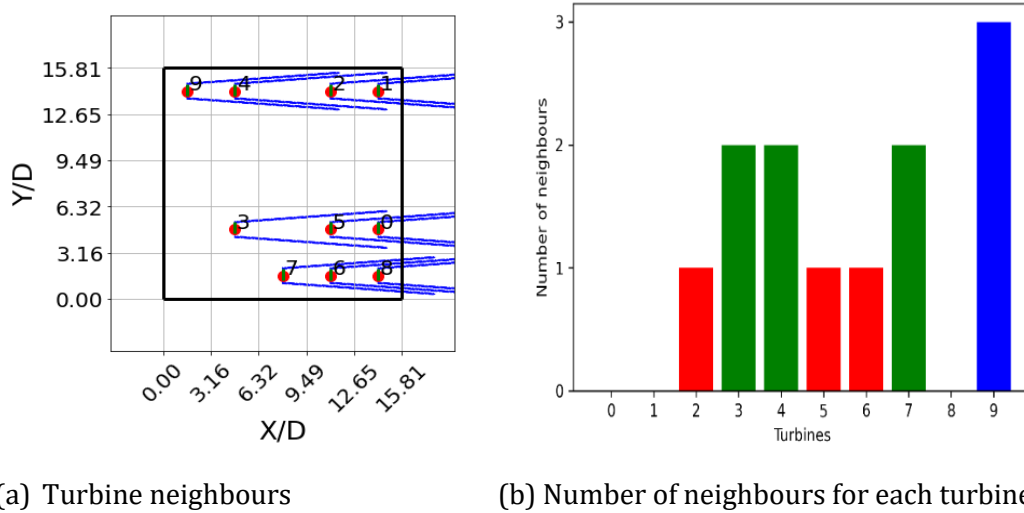


Figure 11: Identified turbine neighbours in the wind farm layout for a wind direction of 270°

Once new neighbours were identified for a given direction, the velocity deficit and recovered wind speeds at each turbine position were estimated (Zhang and Wang, 2009). The process was repeated for all wind directions (the study considered 16 sectors of wind direction), and the total representative power was estimated using the superposition method.

The total velocity deficit at each turbine was required to estimate the representative power. This was calculated using superposition techniques. The details of superposition are discussed in the next section.

## 2.7. Superposition

Superposition is a method used to estimate the net effect of an interested variable caused by multiple dependent stimulants. The same principle is used to estimate the net wind speed of any targeted turbine by considering the multiple interactions of the wake caused by the surrounding turbines. The net velocity deficit at each turbine is estimated after the identification of neighbours for each turbine in the classified wind sectors. Some methods of superposition to estimate the net velocity deficit or regained wind speed are discussed below.

### 2.7.1. Geometric sum

In the geometric sum case, the velocity ratios of upstream and downstream turbines were assumed to be geometrically superposed. The velocity ratio at a particular turbine (for free-stream wind speed) was estimated as a geometric sum of velocity ratios of all the upstream turbines and downstream turbines with wake interactions. This is given by (Shao et al., 2019)

$$\frac{v_i}{v_0} = \prod_j^N \frac{v_{ji}}{v_j}, \tag{2.7.1}$$

where N = total number of upstream turbines,  $i$  = the target turbine,  $v_i$  = inflow wind speed of the target turbine  $i$ ,  $v_j$  = inflow wind speed of the upwind turbine  $j$ ,  $v_{ji}$  = wind speed at turbine  $i$  because of the single wake from the turbine  $j$ , and  $v_0$  = free-stream wind speed.

### 2.7.2. Linear sum

In the linear sum method, the velocity deficits are taken as the basis while estimating the net recovered wind speed at the target turbine. The velocity deficit at a particular turbine (for free-stream wind speed) is estimated as a linear sum of velocity deficits at all upstream turbines and downstream turbines with wake interactions. This is given by (Shao et al., 2019)

$$\left(1 - \frac{v_i}{v_0}\right) = \sum_j^N \left(1 - \frac{v_{ji}}{v_j}\right). \quad (2.7.2)$$

### 2.7.3. Sum of squares

This method is almost similar to the linear sum; however, it accounts for the quadratic sum of the velocity deficits to arrive at the wind speed at the targeted turbine. This is given by (Shao et al., 2019)

$$\left(1 - \frac{v_i}{v_0}\right)^2 = \sum_j^N \left(1 - \frac{v_{ji}}{v_j}\right)^2. \quad (2.7.3)$$

### 2.7.4. Energy balance

The basis for this method is the kinetic energy conservation between upstream turbines and the turbine with wake interactions. It follows the approach of linear summation. This is given by (Shao et al., 2019)

$$v_0^2 - v_i^2 = \sum_j^N (v_j^2 - v_{ji}^2). \quad (2.7.4)$$

All superposition methods except the geometric sum method use the velocity deficit approach to estimate the wind speed at the targeted turbine. The variation in results from all of these methods is not significant. Therefore, the linear sum method was used in the study due to its simplicity.

An example is provided to illustrate the concept. As shown in Figure 12, turbine T3 is in the wake field of turbines T1 and T2. Turbine T4 is in the wake field of T3, underlying the effect of wake fields generated by T1 and T2. The inflow wind speed at T1, T2, T3, and T4 are indicated as  $v_0$ ,  $v_0$ ,  $v_3$ , and  $v_4$ , respectively. The inflow wind speed at T3 is a fraction of the outflow wind speed from T1 and T2.

The wind speed at the targeted turbine, T4, is estimated using the linear sum method as

$$1 - \frac{v_4}{v_0} = \left(1 - \frac{v_{14}}{v_0}\right) + \left(1 - \frac{v_{24}}{v_0}\right) + \left(1 - \frac{v_{34}}{v_3}\right). \quad (2.7.5)$$



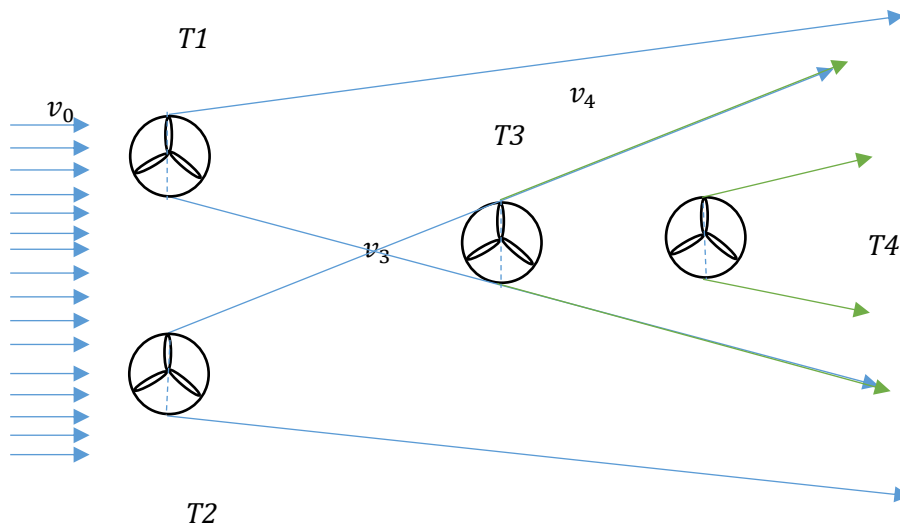


Figure 12: Wake expansion among four turbines

## 2.8. Layout optimisation

### 2.8.1. Layout geometries

The shape of a given land parcel and geography play a significant role while mathematically optimising (positioning the turbines at optimum positions) a wind farm. The first step in layout optimisation is to discretise the land layout into smaller grids. The turbines are positioned inside these grids based on the selected optimisation technique and relevant numerical simulation.

The inputted land area in the model was discretised into square grids because of its simplicity for mathematical simulation. The common rule-of-thumb method is to assign a minimum of  $5 \times D$  (5 times the rotor diameter) space between two turbines. The spacing can be considered less than  $5 \times D$  upon optimisation to nullify the wake effect. Therefore, to start with, the minimum distance between two turbines is considered as  $3 \times D$ . Square grids are developed with a length and breadth of  $5 \times D$ . The available area for movement of each turbine is  $(5 \times D)^2$ .

The optimisation criteria is based on the given farm capacity or land area.

#### Based on farm capacity:

The basis of this approach was wind farm capacity. Using this approach, the number of turbines and the land area were estimated. The details are given below:

Maximum distance between two turbines =  $5 \times D$

Single grid area = Maximum distance between two turbines<sup>2</sup>

Number of turbines =  $\frac{\text{Wind farm capacity}}{\text{Single turbine capacity}}$

Total land area = Number of turbines  $\times$  Single grid area



**Based on a land area:**

The basis of this approach is the land area. The number of turbines in the wind farm is estimated as follows:

$$\text{Number of turbines} = \text{Land area} / \text{single grid area}$$

The study considered different types of geometries for the layout. To illustrate the geometries, a sample case of a wind farm with a farm capacity of 36 MW and a single turbine capacity of 3.6 MW was chosen. A non-dimensional layout was developed using the rotor diameter (D) for this analysis.

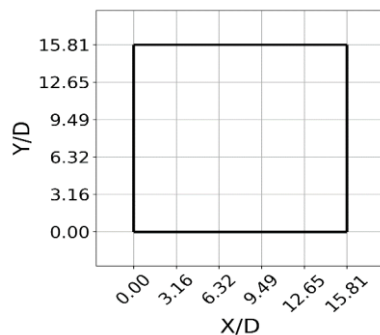
**Square layout**

$$\text{Number of turbines} = \text{Wind farm capacity} / \text{single turbine capacity}$$

$$\text{Total area} = \text{Number of turbines} \times \text{Single grid area}$$

$$\text{Length} = \sqrt{\text{Total area}}$$

$$\text{Breadth} = \sqrt{\text{Total area}}$$



Farm capacity = 36 MW  
 Single turbine capacity = 3.6 MW  
 Total no. of turbines = 10  
 Total area =  $10 \times (5)^2$   
 Length =  $\sqrt{250} = 15.81$   
 Breadth =  $\sqrt{250} = 15.81$

Figure 13: Illustration of the square layout with an example

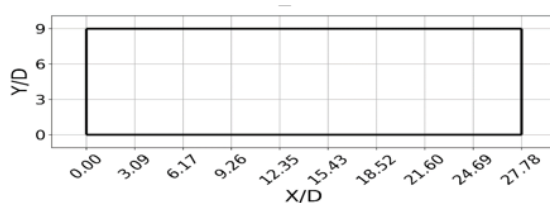
**Rectangle layout**

$$\text{Number of turbines} = \text{Wind farm capacity} / \text{single turbine capacity}$$

$$\text{Total area} = \text{Number of turbines} \times \text{Single grid area}$$

$$\text{Breadth} = \sqrt{\text{No. of turbines}} \times \text{Minimum distance between turbines}$$

$$\text{Length} = \text{Total area} / \text{Breadth}$$



Farm capacity = 36 MW  
 Single turbine capacity = 3.6 MW  
 Total no. of turbines = 10  
 Total area =  $10 \times (5)^2$   
 Breadth =  $\text{int}(\sqrt{10}) \times 3 = 9$   
 Length =  $250/9=27.7$

Figure 14: Illustration of the rectangle layout with an example

**Isosceles triangle**

$$\text{Number of turbines} = \text{Wind farm capacity} / \text{Single turbine capacity}$$

$$\text{Total area} = \text{Number of turbines} \times \text{Single grid area}$$

$$\text{Length} = \sqrt{2 \times \text{Total area}}$$

$$\text{Breadth} = \sqrt{2 \times \text{Total area}}$$



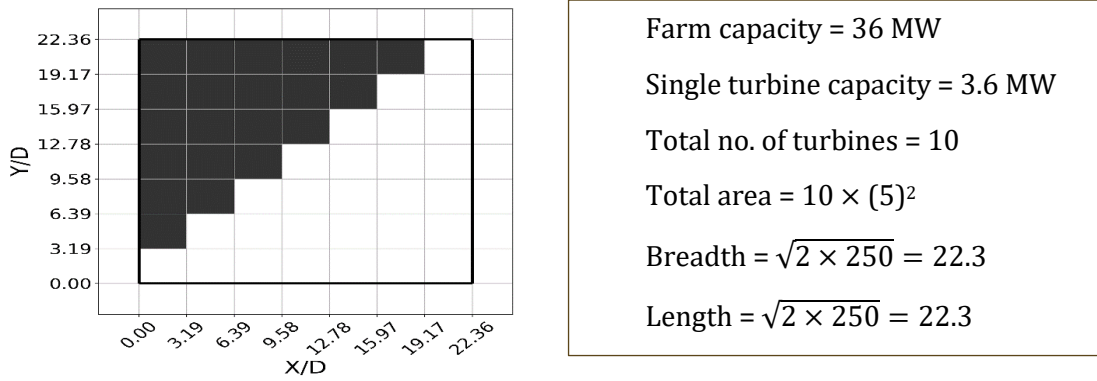


Figure 15: Illustration of the isosceles triangle layout with an example

The space available for positioning the turbines is allocated in the white grids (see Figure 15). The turbines are considered only within the grid boxes, and the edges outside the white grids are discarded for easy numerical calculation.

• **Circle layout**

Number of turbines = Wind farm capacity / Single turbine capacity  
 Total area = Number of turbines × Single grid area

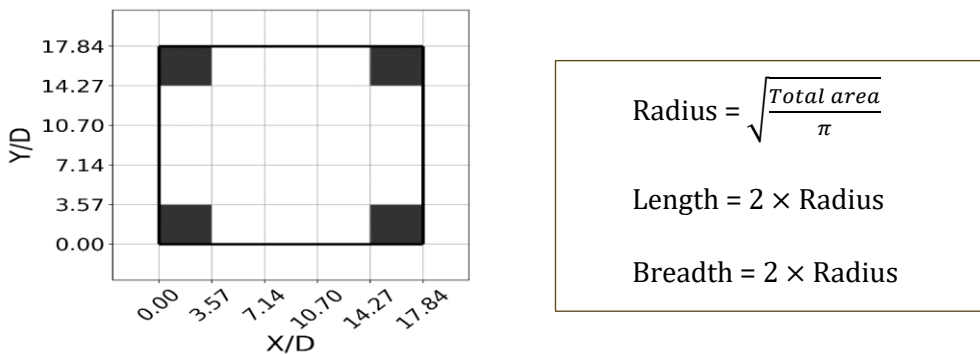


Figure 16: Illustration of the circle layout with an example

**2.8.2. Representative power calculation**

Based on the chosen geometry, turbines are placed within the grids of the layout randomly. The power generated by each turbine and wind farm is estimated. This wake velocity and power are estimated based on representative wind speeds, wind directions, and power curve information, as explained in Section 2.1. The turbines are moved to different grids using a selected optimisation technique and estimate different representative power sets. The optimised layout (turbines siting) is decided based on a layout with maximum representative power. Details about the optimisation methods are discussed in the following section.

**2.8.3. Wind farm layout optimisation**

Optimisation criteria is based on the minimum and maximum power generation at different positions of the turbine in a given layout on an annual basis. This optimisation is crucial for cost minimisation and efficient land utilisation (Barnes and Morozov, 2016; Chen, Li, He, Wang, and Jin, 2015; Song, Chen, He, and Zhang, 2012). Some of the prominent optimisation methods are discussed below.

### a. Genetic algorithm

Genetic algorithm is based on the selection of best chromosomes from the random population by repetition, selection, crossover, and mutation (Mittal, 2010; Mosetti, Poloni, and Diviacco, 1994). The selection process identifies the best possibilities of the items with the desired probability. Crossover generates different items with different probabilities. Mutation randomly selects the better ones and retains the diversity in the probabilities. The algorithm is repeated till the desired condition is met (maximum power generation).

### b. Ant colony algorithm

Ant colony algorithm computationally replicates the behaviour of ants in search of food. This method is a probabilistic way of finding the proper path. In search of food, ants move in colonies and secrete pheromones, a chemical compound that makes them follow a particular path. Based on the quantity of food, the pheromone secreted along the path will get denser. This increases the chance of more ants following the right path and reaching the destination. If there are more probabilistic paths to reach food, ants will eventually choose a path with a shorter distance from the nest by repeating the to and fro motions. Ant density and cycle determine the best probabilistic approach.

### c. Particle swarm optimisation

Particle swarm optimisation is an iterative computational method that is used to arrive at the optimum solution (Mann et al., 2000). The method evolved by mimicking swarm properties of schooling fish or flocking birds (Oliveira, Falcao, Rangel, and Pinto, 2007). The important feature of the particle swarm optimisation topology is the exchange of information with particles. The swarm of particles can be treated as turbines in the wind farm, and its movement in the layout can be used to obtain maximum/optimum energy production with minimum cost.

### d. Monte Carlo optimisation

Monte Carlo (MC) is an evolutionary algorithm to choose the best individuals from a random population in an iterative process. The current study considered MC-based optimisation for the wind farm because of its sophistication.

The Cartesian coordinate system was used in the layout to site the positions of turbines. Initially, turbine positions were set randomly and followed step-by-step to arrive at the maximum energy output and minimum cost. Velocity deficit or the available wind speed for each turbine was estimated for initial turbine positions. Using this, power from all turbines was estimated. However, the total power may not be the maximum energy that can be obtained in the layout. The study defined two important terminologies for performing the MC simulation: *step* and *cycle*.

#### MC steps

In an MC step, turbine positions are displaced randomly each time. The total number of MC steps is equal to the number of turbines in the layout. The displacement of turbines to different cells (square grids) is also random. Random displacement can happen with nine possibilities, that is,  $x = [-1, 0, 1]$  and  $y = [-1, 0, 1]$  at each MC step for each turbine (see Figure 17). The displacement of each turbine will be accepted if it satisfies the acceptance criteria. Thus, all MC steps will be completed. Figure 18 presents the probability of trial displacements of different turbines. As shown, in MC Step 1, the first turbine position is randomly displaced by the neighbouring grid.



The layout power is estimated, and the new turbine position will be considered if it meets the acceptance criteria. In MC Step 2, the displacement of the second turbine takes place. The process of estimating the power and meeting the acceptance criteria continues until the last turbine in the layout to complete all MC steps.

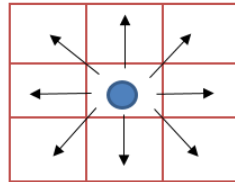
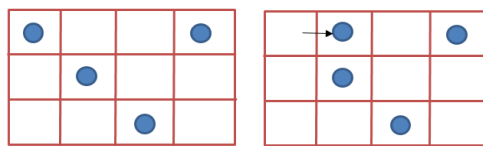


Figure 17: The trial displacement of a turbine within the layout

**The movements of turbines in MC Step 1 can be represented as follows:**



**The movements of turbines in MC Step 2 can be represented as follows:**

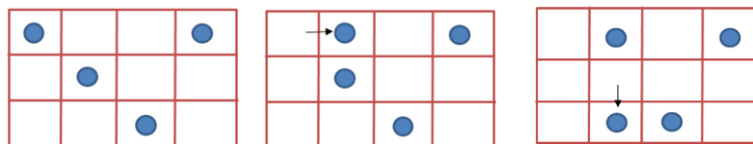


Figure 18: Different MC steps and associated trial displacements

The acceptance criterion used in the simulation is based on the exponential difference in power ( $e^{-\Delta p} > 0$ ) between the previous and current positions of turbines. Further, this acceptance criterion is defined using a random number generator between 0 and 1. If  $\Delta p$  is considerably small, the chance of acceptance probability is large. If the  $\Delta p$  value is high, the probability of acceptance reduces. Figure 19 represents a sample case with a variation of  $\Delta p$  and the acceptance criteria. As seen, if the power difference is higher in the new configuration of the wind farm, the random value will be taken as 1. The random value of 1 indicates the acceptance of the new wind turbines layout (note that the random value of 0 indicates the rejection of the new layout because of no improvement in plant performance) for further optimisation. From the number of MC cycles, the layout with maximum energy output is selected as the optimised layout.

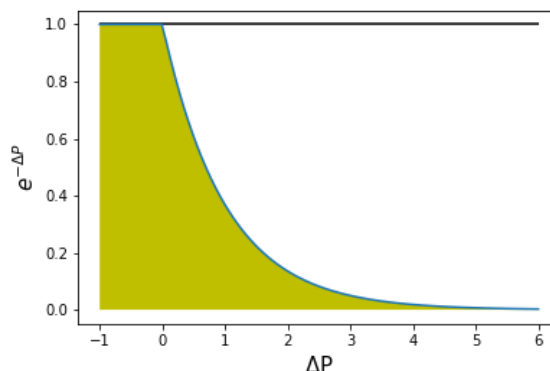


Figure 19: Acceptance criteria of trial displacements

**MC cycles**

The completion of all MC steps is treated as one MC cycle, and it is an input value, which can be decided based on computational power and the desired result. The optimum power generated in the 1st MC cycle (at different displacements) and its corresponding turbine positions will be

the input for the 2nd MC cycle. Similar to the 1st MC cycle, all MC steps will be followed for the 2nd MC cycle to arrive at the optimum power and turbine positions. This process is repeated until the defined number of MC cycles.

## 2.9. Overall flow chart

Figure 20 presents the overall flow chart of the modelling and simulation to estimate the optimum positions of turbines in the wind farm and the techno-economic analysis.

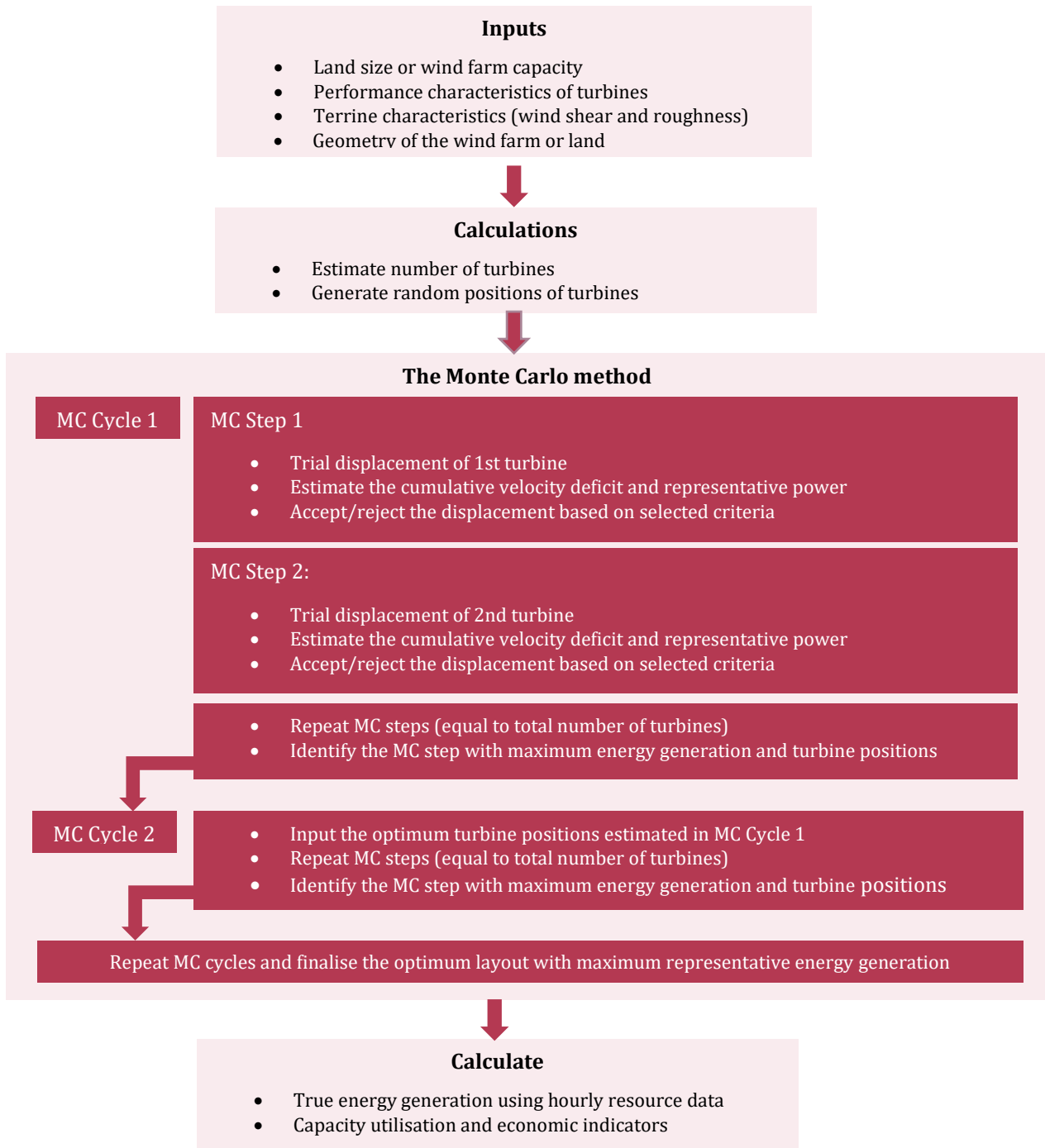


Figure 20: Overall flow chart of the MC simulation







## 3. Results and Analysis: A Case Study

This section discusses the results of the application of the developed model in designing a wind farm in Nagercoil (88.18°N, 77.41°E) as a case study (web tool allows users to choose any desired location). The hourly wind resource data from the National Renewable Energy Laboratory (NREL) were used for the analysis. The study considered a wind farm capacity of 36 MW with 10 turbines, each with a size of 3.6 MW. The hub height and the rotor diameter of each turbine were 90 m and 120 m, respectively. The cut-in and cut-out wind speeds were 3 m/s and 25 m/s, respectively. Key results on the following aspects are presented and analysed in this section:

1. Resource assessment for the chosen location
2. Comparative analysis of different wake models
3. Random positioning of turbines in the chosen shape of the layout
4. Displacement of turbines and representative power using MC steps
5. MC cycles and optimised layout
6. Wake recovery upon optimisation
7. Annual energy output
8. Model validation

### 3.1. Wind resource assessment

A site's potential to set up a wind farm is determined based on wind power density (WPD). WPD is largely a function of wind speed over the year. Historical data are typically used to determine WPD and site potential. Because of limited data availability, the study considered a particular year's (2014) data for the analysis. A wind rose diagram provides information on wind characteristics at a location both in terms of magnitude and direction. Figure 21 presents the wind rose diagram for Nagercoil. The current study considered 16 sectors of wind directions (see Table 1) and nine wind speed bins (see Table 2). Each spoke in the figure indicates how frequently wind blows in different directions with different wind speed intensities (shown in different colour bands). The analysis indicates that wind flows mainly from westerly, WNW, and NNE. These three sectors constitute more than 60% of the total wind (see Figure 21 and Figure 22), with wind speed intensities between 12–15 m/s. Most wind turbines generate rated power at >12 m/s. This indicates that turbines facing westerly, WNW, and NNE directions would generate more power at the chosen location.

The variation of the wind speed in each direction impacts power generation. Therefore, weights were assigned to wind speeds and wind direction (details are indicated in Section 2). The sum of all wind speed weights at each sector was one. Similarly, the sum of the product of wind direction weights and its related sector wind speed weights was also one.

Figure 23 presents a sample case of wind speed variation in select sectors. Table 3 indicates sector weights based on the wind direction over the year with effective wind speeds.



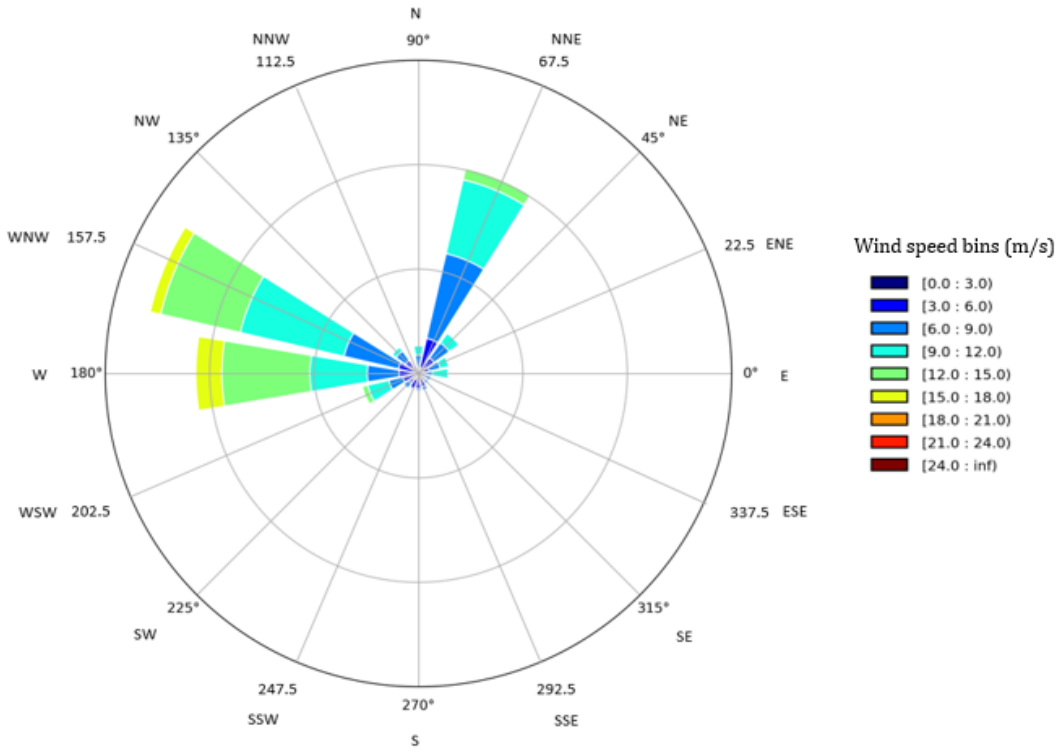


Figure 21: Wind rose diagram for Nagarcoil

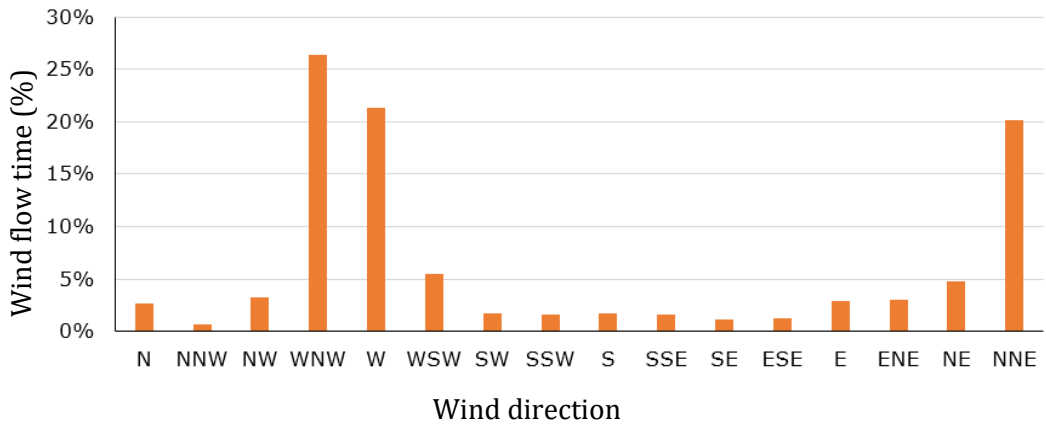


Figure 22: The wind flow distribution in different wind sectors



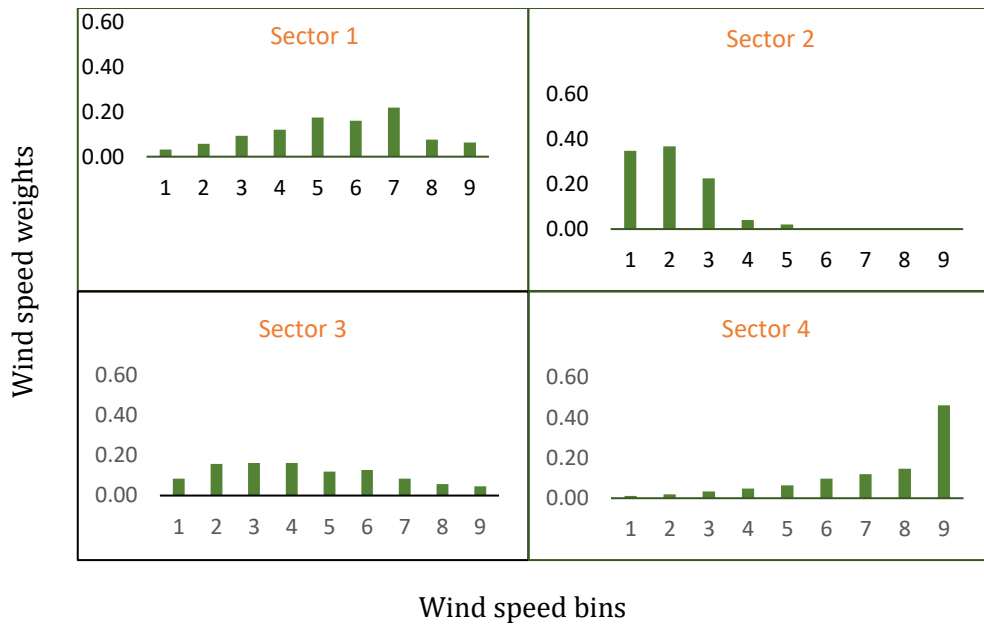


Figure 23: Wind speed bin weights in selected sectors

Table 3: Wind direction sectors and their weights

| Sector | Weight   | Sector | Weight   |
|--------|----------|--------|----------|
| 1      | 0.026826 | 9      | 0.016781 |
| 2      | 0.00708  | 10     | 0.016438 |
| 3      | 0.032078 | 11     | 0.011872 |
| 4      | 0.2638   | 12     | 0.013014 |
| 5      | 0.213    | 13     | 0.02911  |
| 6      | 0.055365 | 14     | 0.030594 |
| 7      | 0.01758  | 15     | 0.037717 |
| 8      | 0.016438 | 16     | 0.201598 |

The weights of the wind speed and wind direction (a total of 144 values) were useful to estimate the representative power of turbines during simulation instead of considering 8760 values in a year. This saves a lot of computational power while optimising a wind farm.

### 3.2. Comparative analysis of different wake models

Wake impacts the power generation from any given turbine, and it needs to be accounted for to estimate the true energy output. The current study considered three wake models to present the wake effect. Jensen and Frandsen follow linear expansion with slight changes in the near and far



wake regions. Bastankhah shows a Gaussian wake expansion and is entirely different from the other two models.

To present the impact of wake, two turbines located at a distance of  $1 \times$  rotor diameter were chosen with different wind speeds. Figure 24 shows the comparison of wake models in terms of regain wind velocities at different positions of wake field behind the rotor. As seen, the wake contracts radially (along y-axis) with equal distribution from the centre of the rotor. Jensen and Frandsen have top hat regains, and Bastankhah follows the Gaussian curve. More wake loss occurs just behind the rotor with a radian wake expansion between -1 and +1. Similarly, Figure 25 presents the variation for an inflow wind speed of 24 m/s. These figures (Figure 24 and Figure 25) indicate that wake effects are minimal when the inflow wind speeds are higher. The study considered the Jensen model for estimation of overlapping wake fields because of its simple mathematical formulae.

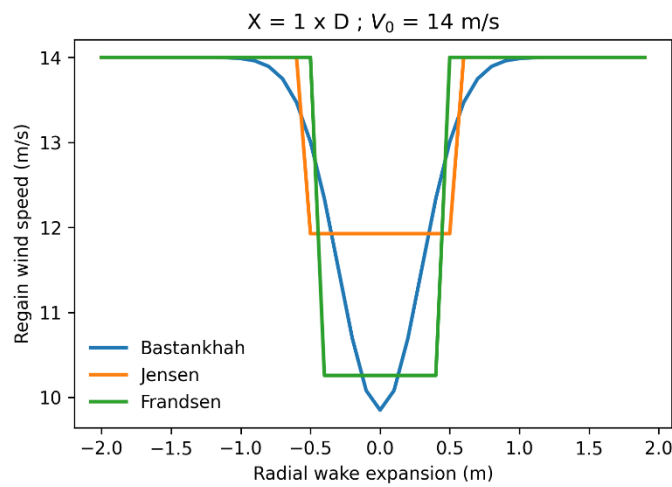


Figure 24: Comparison of different wake models to examine the regain velocity for an inflow wind of 14 m/s

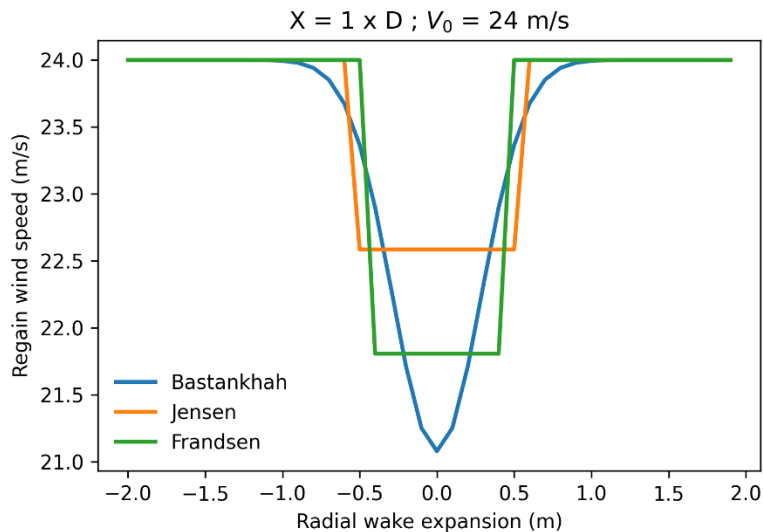


Figure 25: Comparison of different wake models to examine the regain velocity for an inflow wind of 24 m/s

### 3.3. Initial turbine layout configuration

The study considered land with a square shape for illustrating the case study. Figure 26 presents this scenario. The red dots in the figure indicate the position of turbines (generated randomly), and each grid has equal length and breadth. The case is presented below, considering a wind farm capacity of 36 MW.

Farm capacity = 36 MW

Single turbine capacity = 3.6 MW

Total number of turbines =  $\frac{\text{Farm capacity}}{\text{Single turbine capacity}} = 10$

Length of a single grid =  $5 \times D$

Single grid area = Length of a single grid<sup>2</sup>

Area of the layout = Number of turbines  $\times$  Single grid area =  $10 \times (5D)^2$

Length =  $\sqrt{250} = 15.81$

Breadth =  $\sqrt{250} = 15.81$

The total square area was divided into small grids of  $3.16 \times 3.16$  (using the length, breadth, and number of grids in each axis), in terms of rotor diameter, where true dimension of each grid = length or breadth of the farm / length of the single grid.

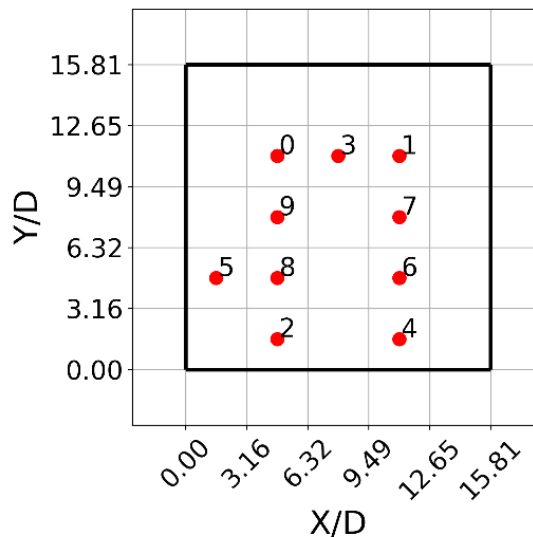


Figure 26: Initial layout of turbines

The area of the layout was discretised with a total number of grids of  $5 \times 5$ , in terms of rotor diameter. However, a minimum distance between turbines of  $3 \times 3$  (in terms of rotor diameter) is considered to have maximum movements of turbines in the layout. The total representative power of the farm was estimated for this initial configuration using equation (2.1.4) along with wake effects. Thus, the evaluated indicative power of the initial layout was 23,000 kW.



### 3.4. Approach for the displacement of turbines

As per the initial layout, 10 turbines were positioned randomly in various grids and their representative power was estimated. A change in the position of turbines might result in an increase or decrease in the overall representative power. Therefore, a systematic procedure, using the Monte Carlo algorithm, was followed for the trial displacement of turbines. According to the flow chart provided in Section 2.9, the position of turbines was moved, considering the MC steps in each MC cycle. From this, positions of turbines corresponding to the optimum representative power were considered as the basis for the next MC cycle. In each cycle, 10 positions of turbines were displaced. An acceptance criteria was used to choose the layout with optimum power. Users can choose the number of MC cycles of interest to run the simulation for obtaining the optimised wind farm layout. The MC cycle iteration repeated until it reached the optimum representative power. Figure 27 indicates the positions of turbines obtained in MC Cycle 1. The corresponding indicative power was 23,170 kW.

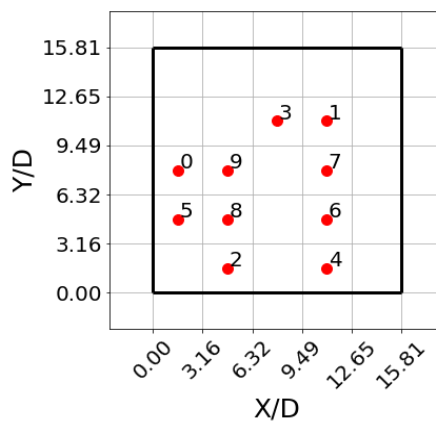


Figure 27: Position of turbines at MC Cycle 1

Figure 28 indicates turbines' positions at MC Cycle 9. Turbine positions were varied in this configuration compared to the initial layout and MC Cycle 1. The indicative power of this configuration was 23,900 kW. An increase of 900 kW of power was observed compared to the initial layout. Figure 29 indicates turbines' positions at MC Cycle 10. This layout resulted in a representative power of 24,000 kW (an increase of 100 kW).

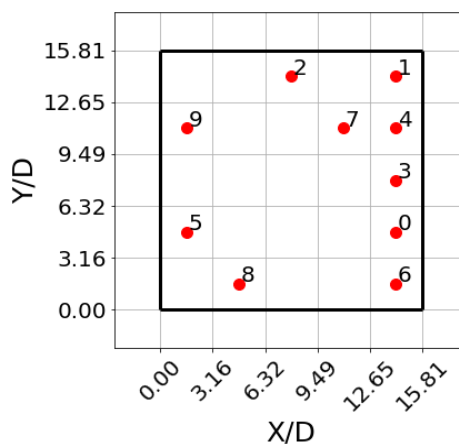


Figure 28: Position of turbines at MC Cycle 9

It was evident that the displacement of turbine positions increases power. The freedom of turbine movements was restricted to an extent within the cells in the discretised layout. Therefore, increasing MC cycles beyond a particular limit will have nil effect on the power increment. Hence, MC cycles was limited to a finite number to reduce computational time.

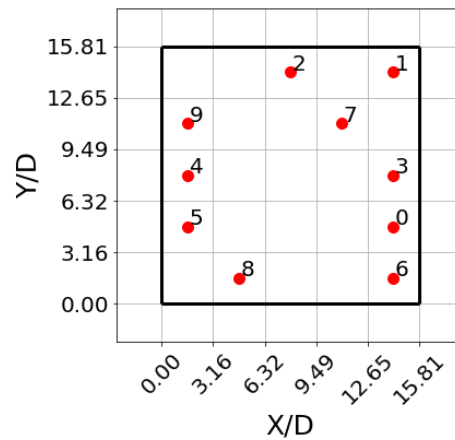


Figure 29: Position of turbines at MC Cycle 10

### 3.5. Optimised farm layout

As indicated in Section 2.8.3, the position of turbines was displaced using MC cycles until optimum power was obtained. The study considered a total of 100 MC cycles to see the improvement in power and observed nil effect beyond a limit. From all the cycles, the layout with maximum power was considered as optimum configuration. Upon simulation, the study arrived at maximum power (24,000 kW) at MC Cycle 10. Figure 30 presents this optimum configuration.

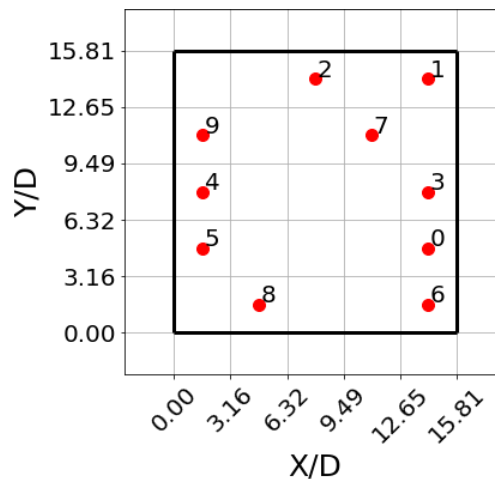


Figure 30: Optimised farm layout

Figure 31 presents the indicative power generated by each turbine at the initial and optimised layout in MC Cycle 1. A significant improvement was seen with the MC simulation.

Figure 32 presents the indicative power of the wind farm for 100 MC cycles. The increment in power beyond the 10th MC Cycle plateaued. It indicates that a higher number of MC cycles may not be significant for a small wind farm. Users have to choose the number of MC cycles



judiciously based on the farm capacity, the number of turbines, and land size to minimise the computational time and cost.

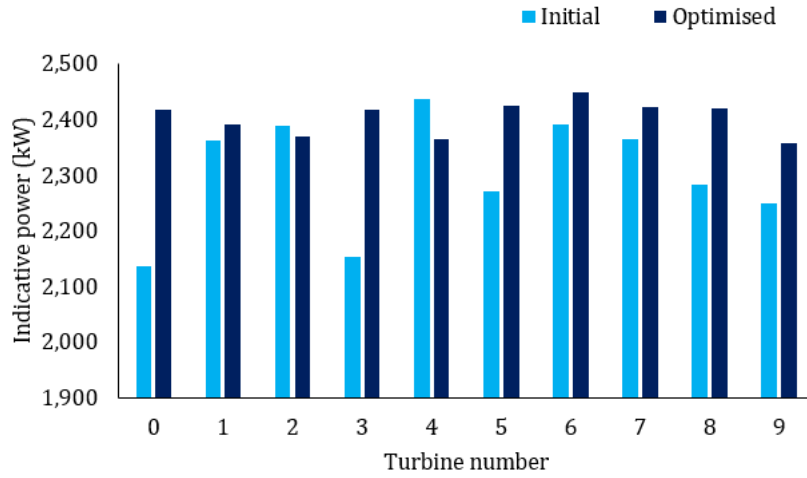


Figure 31: Indicative power of the initial and final layout of MC Cycle 1

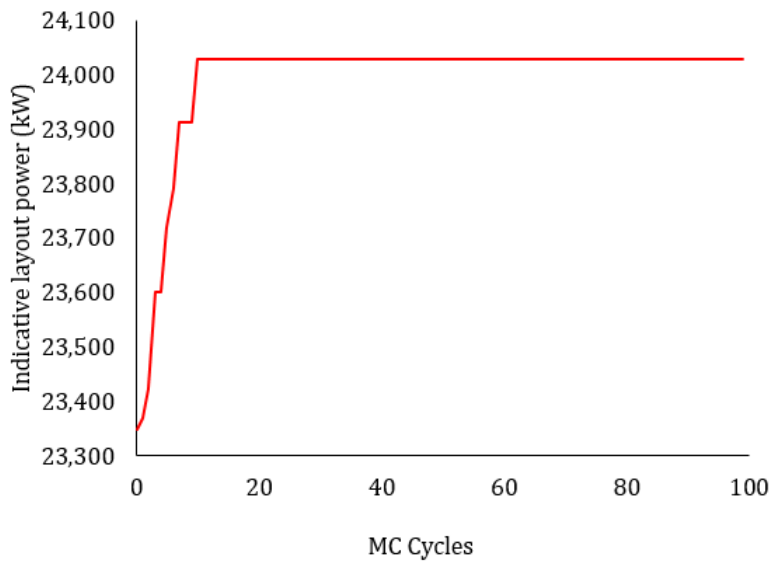


Figure 32: Indicative layout power for 100 MC cycles

### 3.6. Comparison of Initial and Optimised Layout with MC runs

Each MC run performs the displacement of all turbines considering MC cycles and MC steps. Multiple MC runs offer more number of solutions to arrive at the optimum power. In this regard, parallel computing of MC runs would help in optimising the time for simulation. The initial and optimised positions of turbines were different for each MC run because of random positioning, displacement of turbines, and accountancy of wake effects. Figure 33 presents the initial and optimised layout for the first MC run. The maximum indicative power was obtained at MC cycle 10 (see Figure 32). The indicative powers from the initial and optimised layout during the first MC run were 23,000 kW and 24,000 kW, respectively.

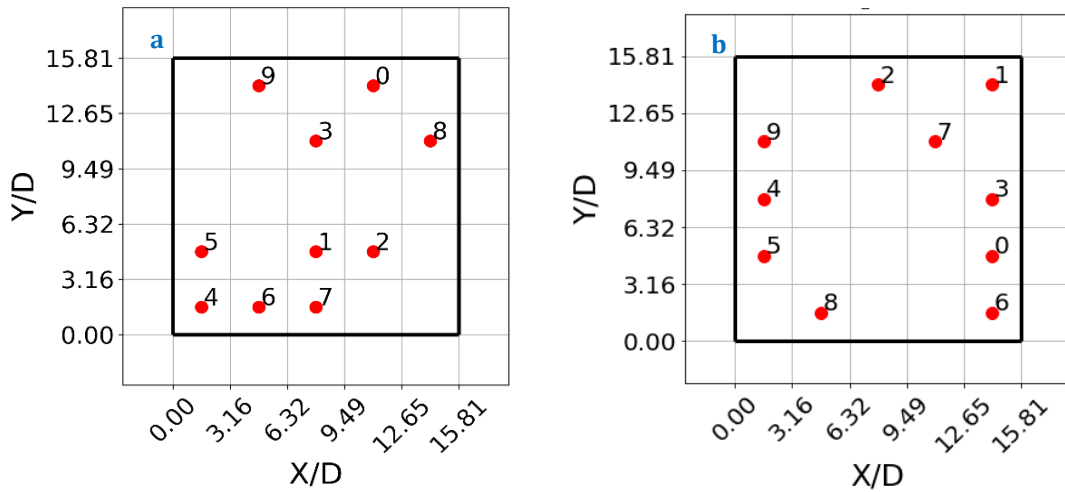


Figure 33: Turbine positioning of initial (a) and optimised layouts (b) for the first MC run

Figure 34 presents the initial and optimised layout of turbine positions for the second MC run. In this case, the maximum indicative power was obtained at the 94th MC cycle (see Figure 35). The indicative powers from the initial and optimised layout during the first MC run were 23,200 kW and 24,000 kW, respectively. In both these MC runs, the indicative powers and turbine positions of the initial layouts were different. However, the indicative powers from the optimised layout were the same but the turbine positions were different. It can be noted that multiple MC runs might offer higher, lower, or equal indicative powers. Among these runs, users have to choose the best configuration that generates maximum power.

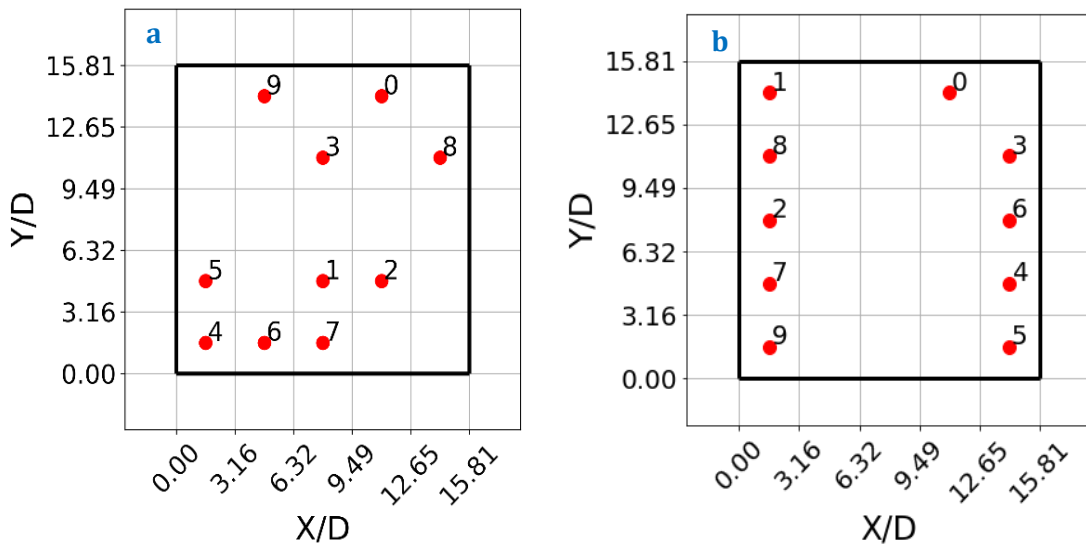


Figure 34: Turbine positioning of the initial (a) and optimised layout (b) for the second MC run



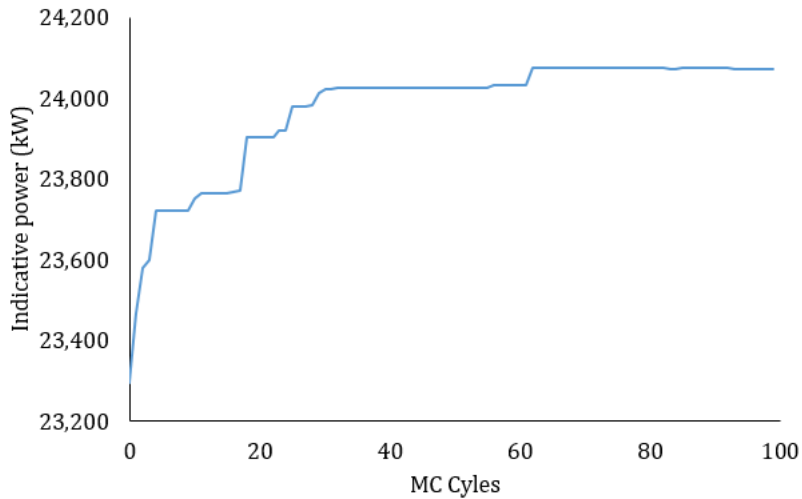


Figure 35: Indicative power output throughout the MC cycles for the second MC run

### 3.7. Comparison of wake recovery

As indicated earlier, the model accounts for wake effects, considering the neighbouring turbines and overlap associated with the wake. Using the Jensen model and the linear sum method of superposition, the net effect of all the turbines was accounted for to estimate the regained wind speed. Figure 36 and Figure 37 present the regained wind speed of all the turbines in different directions for initial and optimised layouts. The wind directions of 308°, 180°, and 31° were considered to illustrate the case. The wake recovery was better in the case of the optimised layout compared to the initial layout. The wake losses reduced to 3% (optimised) from 7% (initial). The same can be witnessed for the indicative power generated by these layouts (refer to Section 2.8.2).

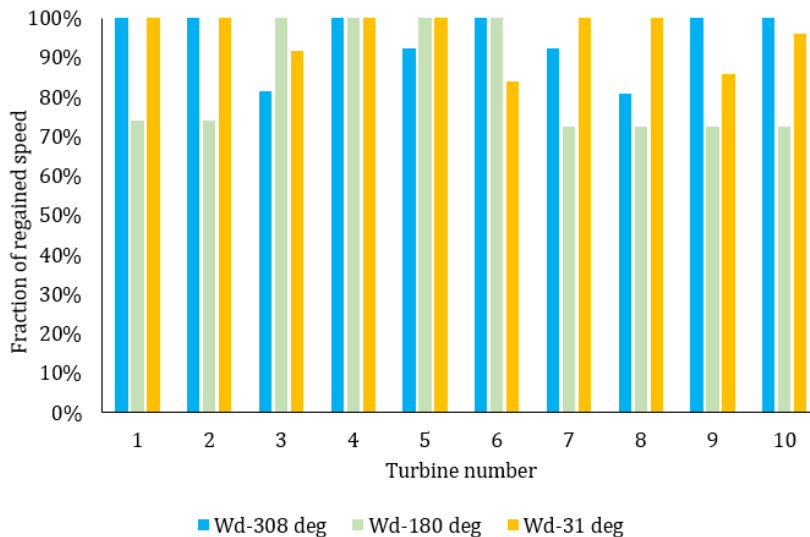


Figure 36: Wake recovery of the initial layout

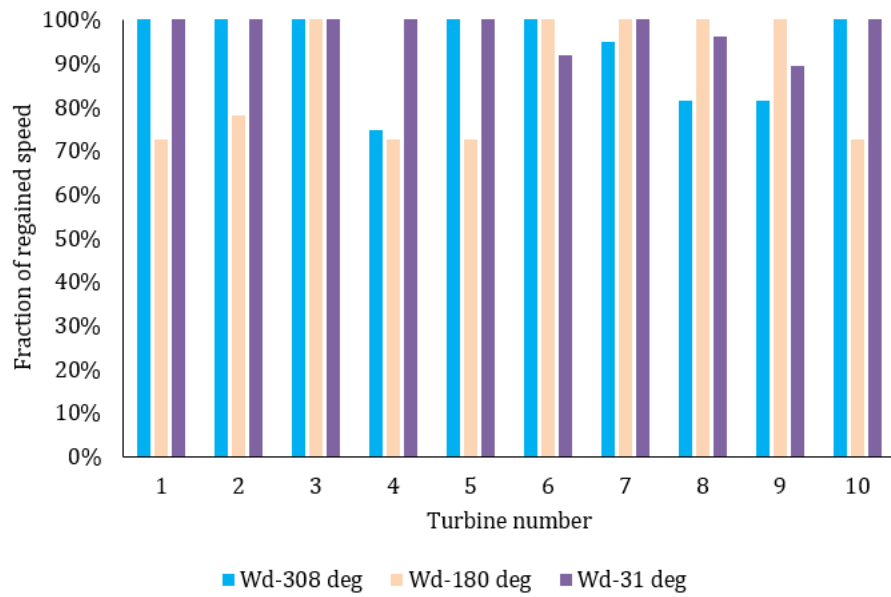


Figure 37: Wake recovery of the optimised layout

### 3.8. Annual electricity of the optimised wind farm

The indicative power was considered to minimise the simulation time while optimising the positions of turbines. The optimised layout was taken as the basis, and the annual electricity generated by the farm, considering hourly resource data (set of wind speed and wind direction), was estimated. Figure 38 presents the electricity generated by each turbine for the initial and optimised layout. The electricity generated by all the turbines in the optimised layout was better compared to the turbines in the initial layout. The annual electricity generated in the initial and optimised layouts was 1,69,000 MWh and 1,77,300 MWh, respectively. The associated plant load factors were 54% and 56%.

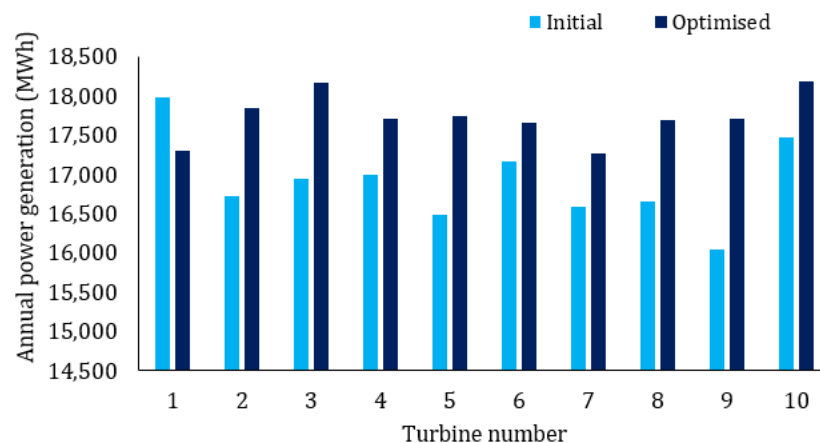


Figure 38: Annual electricity generated by the turbines from the initial and optimised layouts

### 3.9. Economic analysis

A standard levelised cost of electricity (LCOE) model was used to perform the economic analysis (Ramaswamy et al., 2012). LCOE is the ratio of the net present value of the expenses



to the energy. A capital cost of INR 5.92 crore per MW was considered as the basis (Ramesh, 2017). Civil, electrical and grid connection, and planning and miscellaneous were considered as 25%, 17%, and 14% of the capital cost, respectively (IRENA, 2012). For operation and maintenance expenses, 4.5% of the capital cost was accounted. The analysis considers a plant life of 25 years. The estimated net present value of expenses and energy was INR 483 crore and 1,244 million units, respectively. Therefore, the wind farm (36 MW) generated electricity at INR 3.88 per kWh.

### 3.10. Validation of the current model with the System Advisor Model

#### Model

The current model is compared with the System Advisor Model (SAM) for validation. The study considered a total of 32 turbines each with a 3.5 MW capacity (the overall size is 115.2 MW). Table 4 provides the comparison of the current model and SAM.

Table 4: Model validation with SAM

|                                   | Current Study  | SAM                            |
|-----------------------------------|--|--------------------------------|
| Farm capacity (MW)                | 115.2  | 115.2                          |
| Single turbine capacity (MW)      | 3.6  | 3.6                            |
| No. of turbines                   | 32   | 32                             |
| Minimum distance between turbines | 3D (maximum allowance for movement 5D)                       | 5D                             |
| Wake loss                         | 6.6%   | 9.5%                           |
| Annual power output (MWh)         | 2,92,000 (only wake based)<br>2,54,000 (wake + other losses) | 2,53,000 (wake + other losses) |

The comparison was performed in terms of wake losses and the annual electricity generation. The current model was developed considering only wake effects. SAM considers 8D × 8D grid size and accounts for wake effects and other losses such as electrical, plant availability, environmental, and operational aspects. The current model considered 3D × 3D distance between the turbines to allow the maximum number of movements for effective positioning of turbines in the reference farm. Therefore, the comparison was performed considering both scenarios. The current model resulted in lesser wake losses compared to SAM and generated more electricity. However, both models generate nearly the same amount of electricity if all losses are considered.



Figure 39 and Figure 40 present the comparison of optimum turbine positions for the current model and SAM. The current model generated a better layout with turbine positions to account for the wake effects. However, the SAM model positioned the turbines linearly at different distances.

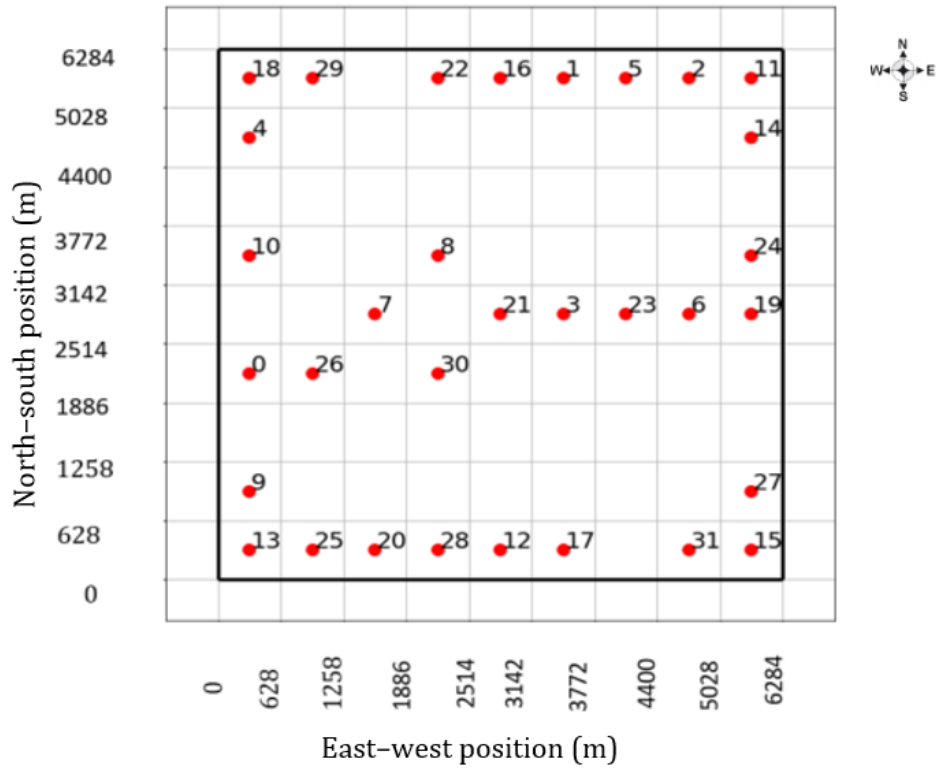


Figure 39: The sample layout from the current model



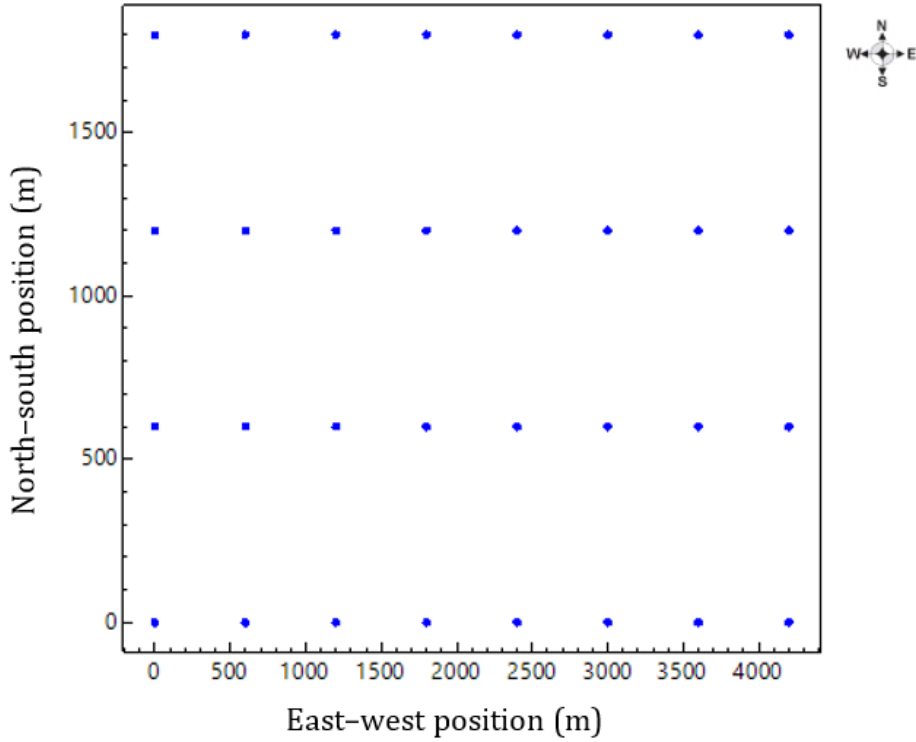


Figure 40: Layout of the sample farm from the SAM model

Also, SAM shows a single line arrangement pattern in case the number of turbines is a prime number. Figure 41 presents this scenario for a wind farm with 13 turbines. It indicates that SAM was eliminating wake effects by positioning turbines at a fixed distance in a single line.

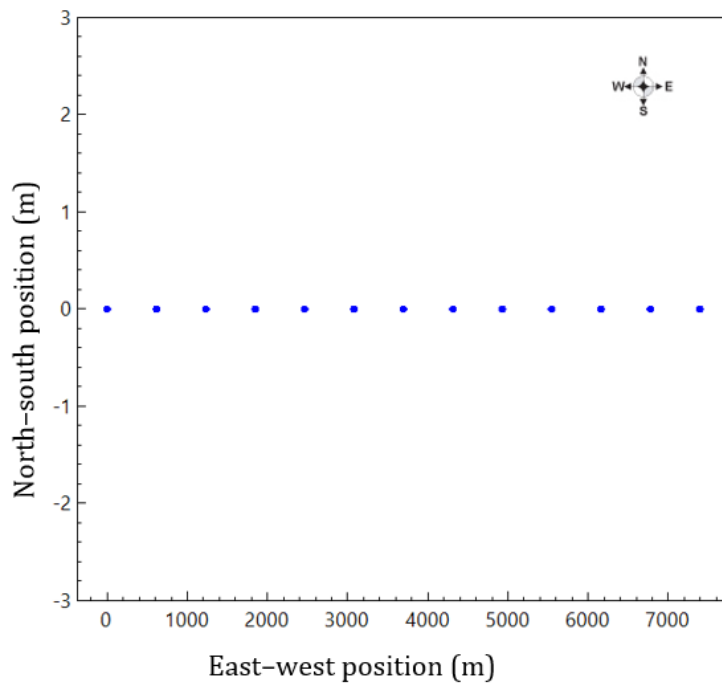


Figure 41: Wind farm layout from SAM for 13 turbines



## 4. Graphical user interface web tool

A graphical user interface (GUI) based web tool was developed based on the model to perform the techno-economic analysis for a range of inputs. Users can provide customised inputs and simulate the tool. The tool provides a variety of results, including resource characteristics, turbine characteristics, wake losses, wind farm optimisation, economic insights to optimise the wind farm, and related economic analysis. Figure 42 provides the sample screen for a resource assessment. This window in the tool enables users to perform resource assessments for default locations and locations of interest (a topographic feature is provided to choose the desired location). So, users can select the location with customised terrain characteristics.

The screenshot shows a web tool interface with a navigation bar at the top containing six buttons: "Resource Assessment", "Turbine characteristics", "Wind farm layout", "Other Inputs", "Economic Model" (highlighted in red), and "Get Results". Below the navigation bar, the "Resource Assessment" section is active. It features a "Location:" dropdown menu set to "Nagercoil", a "Topography:" dropdown menu set to "Open terrain with smooth surface,like concr", and a "Custom upload" checkbox with a "Choose Files" button and "No file chosen" text. The "Location name:" field is "Nagercoil". The "Latitude:" field is "8°11' N", the "Longitude:" field is "77°22' E", and the "Default hub height (m):" field is "40". On the right side, there are two input fields: "Shear:" set to "0.11" and "Roughness (m):" set to "0.0024". A circular arrow icon is visible on the right side of the form.

Figure 42: The sample screen of a resource assessment in the web tool

Figure 43 provides the sample screen for turbine characteristics. The tool allows users to choose default turbines and input relevant details of any chosen turbine. This information will be used along with a power curve to estimate the power generated by the turbine.

The screenshot shows the "Turbine characteristics" section of the web tool. The navigation bar at the top has "Turbine characteristics" highlighted. The "Turbine model and size:" dropdown menu is set to "Siemens Gamesa 3.6 MW". Below it is a "Custom upload" checkbox with a "Choose Files" button and "No file chosen" text. The "Turbine name:" field is "Siemens Gamesa 3.6 MW". The "Rotor diameter (m):" field is "120", the "Hub height (m):" field is "90", and the "Modified hub height (m):" field is "90". A circular arrow icon is visible on the right side of the form.

Figure 43: The sample screen of turbine characteristics in the web tool



Figure 44 provides the sample screen to optimise the wind farm layout. The tool allows users to choose relevant criteria for optimisation based on either land area or wind farm capacity. Users can choose one of these criteria to meet their objective function: maximum utilisation of land to achieve higher installed capacity and electricity production or maximum electricity generation for a given wind farm capacity. The technical optimisation will ensure that power generation happens at a low cost of electricity. Further, users can choose the size of the grid and the minimum distance between turbines to analyse the best scenario. Default wake model options indicated in the web tool are to be considered to estimate the wake loss. The overlap of wakes between turbines can be solved by selecting any desired superposition techniques listed in the tool.

Figure 44: The sample screen of the wind farm layout in the web tool

For optimising of a wind farm using the Monte Carlo method, users need to decide the number of trial displacements of turbines within the area chosen to get maximised electricity generation. Higher number of MC cycles require a long time for computation. . Users can perform parallel runs of the tool for seeing quick performance comparisons and identifying optimum positions of turbines.

Figure 46 and Figure 46 present other sample screens of the tool related to plant availability, losses other than wind wakes, plant life, and economics.

Figure 45: Losses and other wind characteristics incorporated in the tool

Resource Assessment   Turbine characteristics   Wind farm layout   Other Inputs   **Economic Model**   Get Results

Turbines capex (INR Cr/MW):  
 chosen turbine size is **3.6 MW**

Civil works and foundation cost (% of turbines cost):

Planning and miscellaneous cost (% of turbines cost):

Electrical and grid connection cost (% of turbines cost):

Operations and maintenance cost (% of total capex):

Inflation on operations and maintenance (% per year):

Land cost (INR/MW/Year):

Inflation on land lease (% per year):

**Means of finance**

Debt (%):

Equity (%):

**Rate of interest**

Debt (%):

Equity (%):

→

Figure 46: Economic model in the tool

Overall, the tool helps in providing insights on resource assessment, optimum positions of turbines, land-use efficiency, annual electricity generated by a wind farm, capacity utilisation factors, and economic indicators.







## 5. Conclusion

The study presented a detailed engineering and economic modelling to optimise a wind farm at any given location. The model considered wind resource characteristics, different shapes of land, landscape parameters, and wake effects while optimising the wind farm using the Monte Carlo method. A new concept of indicative power was used to minimise the simulation time using effective wind speeds and wind directions. A case study was presented to emphasise the techno-economic results of the application of the developed model for designing a wind farm in Nagercoil. The results are explained in terms of wind potential at a site, performance comparison of wake models, detailed approach to the Monte Carlo method to position turbines, and plant performance (capacity utilisation and generation costs). The case study indicates that the model helps in positioning wind turbines optimally by minimising wake losses (3% wake loss in the optimum layout vs. 7% wake loss in the initial layout) and maximising electricity generation (the optimised layout has a 5% electricity improvement on an annual basis). Results have been validated using a System Advisor Model (SAM). The current model provides better optimised turbine positions by minimising wake losses and utilising land effectively, compared to SAM. Further, a graphical user interface (GUI) web tool was developed for application of the model. This is an interactive simulation tool for users to input customised technical and economic parameters and analyse plant performance.





## 6. References

- Baker, N. F., Stanley, A. P., Thomas, J. J., Ning, A., & Dykes, K. (2019). Best practices for wake model and optimization algorithm selection in wind farm layout optimization. In *AIAA Scitech 2019 forum* (p. 0540). DOI: [10.2514/6.2019-0540](https://doi.org/10.2514/6.2019-0540)
- Balasubramanian, K., Thanikanti, S. B., Subramaniam, U., Sudhakar, N., & Sichelalu, S. (2020). A novel review on optimization techniques used in wind farm modelling. *Renewable Energy Focus*, 35, 84-96. DOI: [10.1016/j.ref.2020.09.001](https://doi.org/10.1016/j.ref.2020.09.001)
- Barnes, R. H., & Morozov, E. V. (2016). Structural optimisation of composite wind turbine blade structures with variations of internal geometry configuration. *Composite Structures*, 152, 158-167. DOI: [10.1016/j.compstruct.2016.05.013](https://doi.org/10.1016/j.compstruct.2016.05.013)
- Bastankhah, M., & Porté-Agel, F. (2014). A new analytical model for wind-turbine wakes. *Renewable energy*, 70, 116-123. DOI: [10.1016/j.renene.2014.01.002](https://doi.org/10.1016/j.renene.2014.01.002)
- Charhouni, N. (2015, August). Qualification of three analytical wake models. In *CFM 2015-22ème Congrès Français de Mécanique*. AFM, Maison de la Mécanique, 39/41 rue Louis Blanc-92400 Courbevoie. URL: <https://core.ac.uk/download/pdf/33523659.pdf>
- Chen, Y., Li, H., He, B., Wang, P., & Jin, K. (2015). Multi-objective genetic algorithm based innovative wind farm layout optimization method. *Energy Conversion and Management*, 105, 1318-1327. DOI: [10.1016/j.enconman.2015.09.011](https://doi.org/10.1016/j.enconman.2015.09.011)
- Frandsen, S., Barthelmie, R., Pryor, S., Rathmann, O., Larsen, S., Højstrup, J., & Thøgersen, M. (2006). Analytical modelling of wind speed deficit in large offshore wind farms. *Wind Energy: An International Journal for Progress and Applications in Wind Power Conversion Technology*, 9(1-2), 39–53. DOI: [10.1002/we.189](https://doi.org/10.1002/we.189)
- Gebraad, P. M., Teeuwisse, F., Van Wingerden, J., Fleming, P. A., Ruben, S., Marden, J., & Pao, L. (2016). Wind plant power optimization through yaw control using a parametric model for wake effects—A CFD simulation study. *Wind Energy*, 19(1), 95–114. DOI: [10.1002/we.1822](https://doi.org/10.1002/we.1822)
- Göçmen, T., Laan, P. van der, Réthoré, P.-E., Diaz, A. P., Larsen, G. Chr., & Ott, S. (2016). Wind turbine wake models developed at the technical university of Denmark: A review. *Renewable and Sustainable Energy Reviews*, 60, 752–769. DOI: [10.1016/j.rser.2016.01.113](https://doi.org/10.1016/j.rser.2016.01.113)
- Gualtieri, G. (2019). A novel method for wind farm layout optimization based on wind turbine selection. *Energy Conversion and Management*, 193, 106–123. DOI: [10.1016/j.enconman.2019.04.059](https://doi.org/10.1016/j.enconman.2019.04.059)
- IRENA. (2012). *Renewable energy technologies: cost analysis series - Wind Power*. URL: <https://www.irena.org/publications/2012/Jun/Renewable-Energy-Cost-Analysis---Wind-Power>
- Jensen, N. O. (1983). *A note on wind generator interaction* (Vol. 2411). Roskilde, Denmark: Risø National Laboratory. URL: [https://backend.orbit.dtu.dk/ws/portalfiles/portal/55857682/ris\\_m\\_2411.pdf](https://backend.orbit.dtu.dk/ws/portalfiles/portal/55857682/ris_m_2411.pdf)
- Kim, H., Kim, K., Bottasso, C. L., Campagnolo, F., & Paek, I. (2018). Wind turbine wake characterization for improvement of the Ainslie eddy viscosity wake model. *Energies*, 11(10), 2823. DOI: [10.3390/en1102823](https://doi.org/10.3390/en1102823)



- Mann, R. F., Amphlett, J. C., Hooper, M. A. I., Jensen, H. M., Peppley, B. A., & Roberge, P. R. (2000). Development and application of a generalised steady-state electrochemical model for a PEM fuel cell. *Journal of Power Sources*, 86(1-2), 173-180. DOI: [10.1016/S0378-7753\(99\)00484-X](https://doi.org/10.1016/S0378-7753(99)00484-X)
- Mittal, A. (2010). *Optimization of the layout of large wind farms using a genetic algorithm* (Doctoral dissertation, Case Western Reserve University). URL: [https://etd.ohiolink.edu/apexprod/rws\\_etd/send\\_file/send?accession=case1270056861&disposition=inline](https://etd.ohiolink.edu/apexprod/rws_etd/send_file/send?accession=case1270056861&disposition=inline)
- Mosetti, G., Poloni, C., & Diviacco, B. (1994). Optimization of wind turbine positioning in large windfarms by means of a genetic algorithm. *Journal of Wind Engineering and Industrial Aerodynamics*, 51(1), 105-116. DOI: [10.1016/0167-6105\(94\)90080-9](https://doi.org/10.1016/0167-6105(94)90080-9)
- Niayifar, A., & Porté-Agel, F. (2015, June). A new analytical model for wind farm power prediction. In *Journal of physics: conference series* (Vol. 625, No. 1, p. 012039). IOP Publishing. DOI: [10.1088/1742-6596/625/1/012039](https://doi.org/10.1088/1742-6596/625/1/012039)
- Oliveira, V., Falcao, D., Rangel, C., & Pinto, A. (2007). A comparative study of approaches to direct methanol fuel cells modelling. *International Journal of Hydrogen Energy*, 32(3), 415-424. DOI: [10.1016/j.ijhydene.2006.06.049](https://doi.org/10.1016/j.ijhydene.2006.06.049)
- Ramaswamy, M., Chandrasekaran, V., Krishnan, R., Thirumalai, N., Suresh, N., Rao, B. S., Dolly, S. K., Kanth, V. C., & Kumar, V. A. (2012). Engineering economic policy assessment of concentrated solar thermal power technologies for India. *Center for Study of Science Technology and Policy*. URL: <https://www.cstep.in/publications-details.php?id=756>
- Ramesh, M. (2017). Gamesa launches 2-MW turbine. *The Hindu Businessline*. URL: <https://www.thehindubusinessline.com/companies/Gamesa-launches-2-MW-turbine/article20393488.ece>
- Shao, Z., Wu, Y., Li, L., Han, S., & Liu, Y. (2019). Multiple Wind Turbine Wakes Modeling Considering the Faster Wake Recovery in Overlapped Wakes. *Energies*, 12(4), 680. DOI: [10.3390/en12040680](https://doi.org/10.3390/en12040680)
- Sizhuang, L., & Youtong, F. (2014, October). Analysis of the Jensen's model, the Frandsen's model and their Gaussian variations. In *2014 17th international conference on electrical machines and systems (ICEMS)* (pp. 3213-3219). IEEE. DOI: [10.1109/ICEMS.2014.7014046](https://doi.org/10.1109/ICEMS.2014.7014046)
- Song, M., Chen, K., He, Z., & Zhang, X. (2012). Wake flow model of wind turbine using particle simulation. *Renewable Energy*, 41, 185-190. DOI: [10.1016/j.renene.2011.10.016](https://doi.org/10.1016/j.renene.2011.10.016)
- Tong, W., Chowdhury, S., Zhang, J., & Messac, A. (2012, September). Impact of different wake models on the estimation of wind farm power generation. In *12th AIAA Aviation Technology, Integration, and Operations (ATIO) Conference and 14th AIAA/ISSMO Multidisciplinary Analysis and Optimization Conference* (p. 5430). DOI: [10.2514/6.2012-5430](https://doi.org/10.2514/6.2012-5430)
- Yang, K., & Cho, K. (2019). Simulated annealing algorithm for wind farm layout optimization: A benchmark study. *Energies*, 12(23), 4403. DOI: [10.3390/en12234403](https://doi.org/10.3390/en12234403)
- Zhang, X., & Wang, W. (2009, March). Wind farm and wake effect modeling for simulation of a studied power system. In *2009 IEEE/PES power systems conference and exposition* (pp. 1-6). IEEE. DOI: [10.1109/PSCE.2009.4839929](https://doi.org/10.1109/PSCE.2009.4839929)





**CENTER FOR STUDY OF SCIENCE, TECHNOLOGY & POLICY**

**Bengaluru**

18, 10<sup>th</sup> Cross, Mayura Street, Papanna Layout,  
Nagashettyhalli, RMV II Stage, Bengaluru 560094  
Karnataka (India)

**Noida**

1<sup>st</sup> Floor, Tower-A, Smartworks Corporate Park, Sector 125,  
Noida 201303, Uttar Pradesh (India)



[www.cstep.in](http://www.cstep.in)



+91-8066902500



[cpe@cstep.in](mailto:cpe@cstep.in)



[@cstep\\_India](https://twitter.com/cstep_India)